A PERTURBATION STUDY OF PARTICLE DYNAMICS IN A PLANE WAKE FLOW

T. J. Burns

Mathematical and Computational Sciences Division, Information Technology Laboratory

National Institute of Standards and Technology, Gaithersburg, MD 20899-8910

R. W. Davis and E. F. Moore

Process Measurements Division, Chemical Science and Technology Laboratory

National Institute of Standards and Technology, Gaithersburg, MD 20899-8360

(November 10, 1998)

We analyze the dynamics of small, rigid, dilute spherical particles in the far wake of a bluff body under the assumption that the background flowfield is approximated by a periodic array of Stuart vortices that can be considered to be a regularization of the von Kármán vortex street. Using geometric singular perturbation theory and numerical methods, we show that when inertia (measured by a dimensionless Stokes number) is not too large, there is a periodic attractor in the phase space of the dynamical system governing the particle motion. We argue that this provides a simple mechanism to explain the unexpected "focusing" effect that has been observed both numerically and experimentally in the far-wake flow past a bluff body by Tang, et al. (1992). Their results show that over a range of Reynolds numbers and intermediate values of the Stokes number, particles injected into the wake of a bluff body concentrate near the edges of the vortex structures downstream, thus tending to "demix" rather than disperse homogeneously.

Key words: particle dynamics, fluid dynamics, wake flows, singular perturbation, invariant manifold

I. INTRODUCTION

The transport of small particles through wakes or mixing layers is a common phenomenon found in many technological and natural flow systems, with applications in such areas as power production and pollution control. The primary feature of both of these types of fluid flows is their arrays of organized vortex structures. Thus, several recent investigations have analyzed particle dynamics in either analytically-defined or numerically-generated vortical flows [5,6,17–20,24,37–39,41].

In dilute wake flows, where the appropriate particle equations of motion are Lagrangian and account for drag only, a particularly interesting effect that has been observed both numerically and experimentally in the wake behind a bluff body over a range of Reynolds numbers is "particle focusing" [37,6]. This refers to the tendency of particles in a certain size range to "demix" or become concentrated (i.e., focused) in narrow bands near the peripheries of the vortex street that forms downstream. This particular self-organizing particle dispersion pattern is not seen in mixing layers, where vortex merging generally occurs [5]. As pointed out in a number of studies (e.g., [21,20]), the key parameter here is the Stokes number **St**, which is the ratio of the aerodynamic response time of a particle to a characteristic flow time. A small Stokes number implies that the particles essentially track with the fluid flow, while a large Stokes number implies large inertial resistance to changes in the flow. In other words, the magnitude of the dissipative drag on a particle in the flow is proportional to the Stokes number. The "focusing" effect has been observed to occur at intermediate Stokes numbers of order one, as shown in Fig. 1 (from [6]). The visualizations here are streakline plots of particles injected with the local flow velocity just downstream of the rear face of a square during the course of a Navier-Stokes simulation of unsteady two-dimensional laminar flow at a Reynolds number of 100 [7,8]. As can be seen, the effect of Stokes number on these visualizations is quite striking.

By studying instantaneous streamline patterns at selected phases in vortex-shedding cycles using a variety of flow visualization techniques, Perry, Chong, and Lim [28] identified two different regimes in the flow behind a bluff body for a Reynolds number on the order of 100. In the closest, the "near-wake" region of a cylinder that starts from rest, there is a cavity that starts out closed but opens as the vortex shedding process sets in behind the body. Once this happens, "instantaneous alleyways" form connecting the flow in the cavity with that downstream. More recent work by a number of groups, in particular Shariff, Pulliam, and Ottino [33], Sommerer, Ku, and Gilreath [34], Duan and Wiggins [10], and Sommerer, Ott, and Tél [35], shows that complex fluid mixing takes place in the cavity directly behind the body. In fact, various measurements by Sommerer, et al. [34] support the hypothesis that there is a "chaotic saddle" [26] in this region. A little further downstream, in what Perry, Chong, and Lim call the "far wake", vortex shedding sets up a steady-state oscillation in the flow behind the bluff body, with period equal to the time between formation of successive staggered pairs of vortices. It is in this "far-wake" regime that the "particle-focusing" phenomenon has been observed in numerical and experimental studies.

Motivated by Aref and Pomphrey's [3,2] result that, in general, a system of more than three point vortices in an unbounded two-dimensional region is chaotic, Tang, et al. [37] computed the correlation dimension d_G [13] for particle dispersion as part of some inviscid discrete vortex simulations of a plane wake flow downstream of a bluff body. They found that $d_G = 1.40$ for $\mathbf{St} = 0.01$, $d_G = 1.00$ for $\mathbf{St} = 1$, and $d_G = 1.43$ for $\mathbf{St} = 10$. Thus, they found a fractal correlation dimension for values of the Stokes number far from unity. However, at least for larger-scale features of the particle flows, they found a non-fractal correlation dimension of one when the Stokes number is order one and the "focusing" effect is most pronounced. This suggests the presence of a one-dimensional attractor in the dynamical system governing the particle motion. Notwithstanding the complicated fluid kinematics in the "near-wake" regime, such an attractor is typically not associated with chaotic dynamics. The purpose of this paper is to show, in as simple a setting as possible, that for values of the Stokes number that are not too large, such an attractor is to be expected in the dynamical system of the particles in the "far-wake" vortex street region. Thus, this provides a plausible explanation for the observed focusing effect in the wake of a bluff body.

II. FORMULATION

We will investigate particle focusing by means of a perturbation analysis of particle dynamics in a simple model of a plane wake flow, with emphasis on a discussion of dispersion. The perturbation parameter, ϵ, is a coefficient that is smaller than but directly proportional to the Stokes number $\mathbf{St}$. The analysis we present here follows the approach used in the related study of Rubin, Jones, and Maxey [29] of particle motion in an analytically-defined cellular flowfield.

As is clear from some of the photographs in Perry, Chong, and Lim ([28], Figs. 6 (a) & 7), for Reynolds numbers that are of the order of 100, the regular vortex pattern in the far wake persists downstream a distance of many vortex spacings, so that it is approximately periodic in space as well as time over a significant distance. (Additionally, see the visualizations of experimental laminar wakes in Van Dyke [40], Figs. 94, 95, 96, and 98; in particular, note the uniform vortex spacing in these figures.) Thus, at relatively low Reynolds number, even though actual wake flows will have differing characteristics due to variations in flow parameters, von Kármán's vortex street, a mathematical idealization in which staggered point vortices move at constant speed and separation without the lateral spreading and eventual breakup seen in actual wake flows (see, e.g., [16,23]), is an acceptable approximation to the vortex pattern observed in laminar wake flows past bluff bodies (also see Milne-Thomson [23], Saffman and Schatzman [32], and Saffman [31]). For this reason, the flowfield model we employ for the far-wake vortex street behind a bluff body is a regularization of the von Kármán vortex street. Our modification of the von Kármán street, which is presented in Section III, follows Stuart's [36] regularization of a single row of vortices. As far as we know, this regularization was first employed in a particle study by Meiburg and Newton [22], who investigated the motion of passive particles (i.e., without inertia) in a row of point vortices that evolved in time due to viscosity. Subsequently, Tio and co-workers [38,39] performed studies of particle dynamics as a function of several parameters in a periodic row of Stuart vortices. By including the effects of gravity, Tio, et al. found interesting bifurcations to periodic oscillations of various amplitudes in their model. More recently, a related model has been studied by Haffner [14] using geometric singular perturbation theory in an analysis similar to that presented here.

In Section IV, we begin our investigation of dilute particle motion in the analytically-defined vortex street flowfield. A center manifold construction, based on Fenichel's geometric singular perturbation theory [12,15,43], is used to show that after an initial transient behavior, the four-dimensional position-velocity phase flow of the system reduces to what is essentially a two-dimensional motion on a cylinder. This useful mathematical result allows us to conclude immediately that an attractor with fractal dimension is not possible in this situation. The center manifold reduction also allows us to approximate the motion of dilute particles by the motions of corresponding material points in a small perturbation of the regularized von Kármán street vector field in an easily visualized two-dimensional phase space. This is the subject of Section V, where the particle motion on the center manifold is studied using numerical methods. Such an analysis, which would be extremely difficult to perform in the original four-dimensional phase space, provides much more detailed information about the particle motion than can be obtained by direct numerical simulation of the original system of equations [7,8]. In particular, the qualitative features of the flow on the two-dimensional center manifold can be studied in detail, including properties of any critical points and the domains of attraction of any attractors in the system.

Our analysis in Section V supports the hypothesis that the focusing of dilute particles in laminar wake flows past a bluff body is the result of nonchaotic dissipative evolution to a one-dimensional attractor that occurs on several different time scales. The flowfield behind the bluff body is approximated in the far wake by a velocity field that is periodic in time with the vortex-shedding period, and periodic in space with the vortex-spacing period. In coordinates that move at the velocity of this associated regularized von Kármán street, particles are initially attracted very rapidly to a center manifold on an order ϵ^{-1}

time scale. After this initial transient behavior, the motion of each particle is close to the motion of a corresponding material point in the center manifold. The resulting behavior can be visualized as the motion of material points in a two-dimensional configuration space for a time-independent, spatially-periodic flow that is a small perturbation of the original von Kármán vortex street flow. Thus, according to our model, the essential particle behavior is governed by a dissipative, autonomous vector field that is periodic in the coordinate parallel to the motion of the street. For values of ϵ that are not too large, particles that start inside each vortex region spin out (in opposite directions because the vortices alternate in sense) at a rate that depends on the size of ϵ, and then enter the region of an undulating jet between the vortices, corresponding to what Perry, Chong, and Lim [28] call an "instantaneous alleyway". For $\epsilon \lesssim 0.25$, there is a unique periodic solution within the region of the jet corresponding to a balance between opposing inertial and dissipative effects. The periodic undulating orbit attracts the particles on a slower time scale that also depends on ϵ. For $\epsilon \approx 0.25$, a bifurcation takes place in the qualitative behavior of the perturbed two-dimensional wake flow. There is no longer an undulating jet region, and the particles are ejected from the street entirely, thus eliminating the periodic attractor. Therefore, rather than a complex bifurcation sequence as a function of Stokes number as Tio, et al. [38] have found in their study of particle motion in a single row of Stuart vortices, a periodic attractor of approximately constant maximum amplitude exists for Stokes numbers that are not too large. This attractor simply ceases to exist beyond a critical Stokes number.

We argue that, because the flowfield in the far wake is well-approximated by a periodic flowfield similar to the one we analyze, the same type of attracting mechanism will exist in a real wake flow. Since a vortex street behind a bluff body does not persist indefinitely in the far wake of a real flow, it follows that there is a range of intermediate values of $\mathbf{St}$, neither too small nor too large, for which the particle-focusing effect is observed either experimentally or numerically. For this range of intermediate values of $\mathbf{St}$ (or ϵ), particles spin out to the attractor within the coherent far-wake region and thus are clearly identifiable as being focused. We also point out in Section V that this effect is most pronounced when the Stokes number is order one. Concluding remarks are given in the final section.

III. BACKGROUND FLOWFIELD

The von Kármán vortex street (see, e.g., Lamb [16] or Milne-Thomson [23]) consists of two parallel staggered infinite rows of counterrotating point vortices of strength κ. The vortex centers in each row are distance a apart, and the two rows are separated by distance b. The rows are assumed to lie parallel to the y_1-axis, with the upper row at $y_2 = b/2$ with strength κ, and the lower row at $y_2 = -b/2$ with strength $-\kappa$. It can be shown [23] that both rows advance in the positive y_1-direction at speed

$$c_1 = \frac{\kappa\pi}{a} \tanh \frac{\pi b}{a}. \tag{1}$$

If a vortex on the upper row lies at $(0, b/2)$ at $t = 0$, the von Kármán vortex street can be defined by the stream function (see, e.g., Milne-Thomson [23])

$$\begin{aligned}\psi(y_1,\, y_2, t) = \frac{1}{2}\,\kappa \Bigg\{ \ln \left[\frac{1}{2} \cosh \left(\frac{2\pi\,(y_2 - b/2)}{a} \right) - \frac{1}{2} \cos \left(\frac{2\pi\,(y_1 - c_1\,t)}{a} \right) \right] \\ - \ln \left[\frac{1}{2} \cosh \left(\frac{2\pi\,(y_2 + b/2)}{a} \right) + \frac{1}{2} \cos \left(\frac{2\pi\,(y_1 - c_1\,t)}{a} \right) \right] \Bigg\},\end{aligned} \tag{2}$$

and the associated time-dependent velocity field is given by

$$\boldsymbol{u}(\boldsymbol{y}, t) = (u_1(y_1, y_2, t), u_2(y_1, y_2, t)) = (-\partial\psi/\partial y_2,\ \partial\psi/\partial y_1). \tag{3}$$

A well-known difficulty with using either (2) or (3) in numerical simulations is the presence of singularities at the vortex centers. In the present study, we will regularize the von Kármán model by following Meiburg and Newton [22], who studied the effects of viscous decay on the motion of passive particles in a single row of corotating vortices using a model based on Stuart's [36] one-parameter family of solutions of the Euler equations in two dimensions (also see Tio, et al. [39], Marcu and Meiburg [17], Marcu, Meiburg, and Raju [19], and Haffner [14]). Thus, the stream function at $t = 0$ of a periodic array of point vortices is modified by introducing a parameter K that controls the distribution of vorticity,

$$\tilde{\psi}(y_1,\, y_2) = \frac{aU_\infty}{2\pi}\, \ln\left[\cosh\left(\frac{2\pi\, y_2}{a}\right) - K\cos\left(\frac{2\pi\, y_1}{a}\right)\right]. \tag{4}$$

Here, U_∞ is the speed of the free stream, a is the spacing between adjacent vortices, and $0 \le K \le 1$. Stuart [36] has shown that $\tilde{\psi}$ satisfies the inviscid vorticity equation $\nabla^2\psi = \omega(\psi)$, where the vorticity is given by

$$\omega\left(\tilde{\psi}\right) = \frac{2\pi\, U_\infty}{a}\left(1 - K^2\right)\exp\left(\frac{-K\,\pi\,\tilde{\psi}}{a\,U_\infty}\right). \tag{5}$$

When $K = 0$, the motion associated with (4) reduces to a hyperbolic tangent shear layer, whereas when $K = 1$, the associated motion becomes a periodic array of point vortices.

Similarly, we modify the stream function (2) by introducing a parameter K, $0 \le K \le 1$,

$$\begin{aligned}\psi_K(y_1,\, y_2, t) = \frac{1}{2}\,\kappa\, \Bigg\{ &\ln\left[\frac{1}{2}\cosh\left(\frac{\pi\,(2y_2 - b)}{a}\right) - \frac{1}{2}\,K\cos\left(2\frac{\pi\ (y_1 - c_K\, t)}{a}\right)\right] \\ &- \ln\left[\frac{1}{2}\cosh\left(\frac{\pi\,(2y_2 + b)}{a}\right) + \frac{1}{2}\,K\cos\left(2\frac{\pi\ (y_1 - c_K\, t)}{a}\right)\right]\Bigg\}.\end{aligned} \tag{6}$$

Each row moves in the positive y_1-direction with speed

$$c_K = \frac{\kappa\pi\sinh\left(2\pi b/a\right)}{a\left[\cosh\left(2\pi b/a\right) + K\right]}, \tag{7}$$

that approaches Eq. (1) as $K \to 1$. For $K = 0$ the motion reduces to a horizontal shear layer defined by a difference of hyperbolic tangents in y_2, while for $K = 1$ the model again becomes the von Kármán vortex street with two periodic rows of point vortices. We note that, because the two-dimensional Euler equations are nonlinear, the associated flow corresponding to the superposition of two regularized counterrotating rows of vortices is no longer a one-parameter family of solutions of these equations.

We now nondimensionalize lengths by half the vertical vortex spacing, $b/2$, and time by the length scale divided by the speed of the street, $b/(2c_K)$, retaining the same notation. This gives the dimensionless stream function

$$\begin{aligned}\psi_K(y_1,\, y_2, t) = {} & \frac{a}{\pi b}\frac{\left[\cosh\left(2\pi b/a\right) + K\right]}{\sinh\left(2\pi b/a\right)} \\ & \times \Bigg\{ \ln\left[\frac{1}{2}\cosh\frac{\pi b}{a}\left(y_2 - 1\right) - \frac{1}{2}\,K\cos\frac{\pi b}{a}\left(y_1 - t\right)\right] \\ & - \ln\left[\frac{1}{2}\cosh\frac{\pi b}{a}\left(y_2 + 1\right) + \frac{1}{2}\,K\cos\frac{\pi b}{a}\left(y_1 - t\right)\right]\Bigg\}.\end{aligned} \tag{8}$$

For specificity, we assume in what follows that the ratio b/a is determined by von Kármán's vortex spacing (see, e.g., Milne-Thomson [23]),

$$\cosh \pi b/a = \sqrt{2}, \tag{9}$$

so that the speed of the street (7) is given by

$$c_K = \frac{2\sqrt{2}\,\kappa\,\pi}{a\,(3+K)}. \tag{10}$$

Transforming to coordinates that move horizontally at the (dimensionless) vortex velocity,

$$\xi_1 = y_1 - t, \qquad \xi_2 = y_2, \tag{11}$$

the stream function of the fluid flow can be written in the autonomous form (i.e., with no explicit dependence on time; see, e.g., Ottino [27]),

$$\begin{aligned} \Psi_K(\xi_1, \xi_2) = \frac{\sqrt{2}\,(3+K)}{4\alpha} & \{\ln\left[\cosh \alpha\,(\xi_2 - 1) - K \cos \alpha\xi_1\right] \\ & - \ln\left[\cosh \alpha\,(\xi_2 + 1) + K \cos \alpha\xi_1\right]\} + \xi_2, \end{aligned} \tag{12}$$

where

$$\alpha = \cosh^{-1} \sqrt{2}. \tag{13}$$

In the moving frame (11), the vortices are stationary relative to a free stream moving to the left at dimensionless speed one.

Thus, the background vortex flowfield is defined by the time-independent Hamiltonian

$$H_K(\xi_1, \xi_2) = -\Psi_K(\xi_1, \xi_2), \tag{14}$$

so that the streamlines of the flow correspond to orbits (i.e., pathlines) of solutions of the corresponding Hamiltonian equations of motion. In more detail, the fluid velocity is given by

$$-\frac{\partial \Psi_K}{\partial \xi_2}(\xi_1, \xi_2) = U_K(\xi_1, \xi_2), \tag{15}$$

$$\frac{\partial \Psi_K}{\partial \xi_1}(\xi_1, \xi_2) = V_K(\xi_1, \xi_2), \tag{16}$$

where

$$\begin{aligned} U_K(\xi_1, \xi_2) = \frac{\sqrt{2}\,(3+K)}{4} \biggl(& \frac{-\sinh \alpha\,(\xi_2 - 1)}{\cosh \alpha\,(\xi_2 - 1) - K \cos \alpha \xi_1} \\ & + \frac{\sinh \alpha\,(\xi_2 + 1)}{\cosh \alpha\,(\xi_2 + 1) + K \cos \alpha \xi_1} \biggr) - 1, \end{aligned} \tag{17}$$

$$\begin{aligned} V_K(\xi_1, \xi_2) = \frac{\sqrt{2}\,(3+K)}{4} \biggl(& \frac{K \sin \alpha \xi_1}{\cosh \alpha\,(\xi_2 - 1) - K \cos \alpha \xi_1} \\ & + \frac{K \sin \alpha \xi_1}{\cosh \alpha\,(\xi_2 + 1) + K \cos \alpha \xi_1} \biggr). \end{aligned} \tag{18}$$

Thus, the relevant autonomous Hamiltonian system for the background flowfield is

$$\frac{d\xi_1}{dt} = \frac{\partial H_K}{\partial \xi_2}(\xi_1, \xi_2) = U_K(\xi_1, \xi_2), \tag{19}$$

$$\frac{d\xi_2}{dt} = -\frac{\partial H_K}{\partial \xi_1}(\xi_1, \xi_2) = V_K(\xi_1, \xi_2). \tag{20}$$

For $0 < K \leq 1$, the equilibrium points of the system (19)–(20) on each row consist of centers (saddles) separated by saddles (centers) at integral (integral plus one half) values of ξ_1 on the upper (lower) row. Each vortex center is surrounded by closed periodic solutions. However, the qualitative properties of the cellular structure created by the vortex rows change at a value of K approximately equal to 0.3. This is shown in Fig. 2, where the separatrices, i.e., the level curves of Ψ_K that pass through the saddle points, are plotted for $K = 0.25,\ 0.2991$, and 0.35. For values of $K < 0.2991$, there is a jet moving to the right between two rows of "Kelvin cat eyes," so that each vortex is isolated from the others by a pair of separatrices. Streamlines corresponding to $K = 0.25$ are depicted in Fig. 3. For $0.3 < K \leq 1$, however, the interaction of the two rows is strong enough that the flowfield takes on the characteristics indicated in Fig. 4, which gives streamlines corresponding to $K = 0.99$. Each vortex is now isolated from the others by a single separatrix, and there is a spatially-periodic jet moving to the left that undulates between and around adjacent vortices. Notice the close similarity of the case $K = 0.99$ to the case of the unmodified von Kármán street ($K = 1$), shown in Fig. 5. Thus, whenever it is necessary to specify a value of K, we will choose $K = 0.99$.

In order to interpret the results in the remainder of the paper, it is helpful, following Perry, Chong, and Lim [28], to view the background flowfield with respect to three different observers. First, suppose the vortices move to the left at speed c_K (dimensionless speed 1) relative to a free stream that also moves to the left at a speed of U_∞ (dimensionless speed $U^* = U_\infty/c_K > 1$). Then, with respect to an observer moving with the free stream, the vortices move to the right at a dimensionless speed of one, with a time-dependent velocity flowfield defined by the potential (8) in the moving $y_1 - y_2$ coordinates. The streamlines at $t = 0$ are given in Fig. 6. As discussed by Perry, Chong, and Lim [28], this flow pattern is often mistakenly described as a representation of the flow with respect to an observer moving with the vortices (see, e.g., the caption to Fig. 98 in Van Dyke [40]). We have already discussed the view as seen by an observer moving with the vortices and thus slower than the free stream. The background flowfield is autonomous, and the free stream moves to the left at a dimensionless speed equal to one (see Fig. 4). Finally, assume for simplicity that $U^* \geq 2$. Then to an observer moving to the left at a dimensionless speed of $U^* - 2$ and thus slower than both the free stream and the street, the free stream appears to move to the left at a speed of two, while the vortices appear to move to the left at a speed of one. The streamlines at $t = 0$ in this nonautonomous case are depicted in Fig. 7, which corresponds to Fig. 5 (f) in Perry, Chong, and Lim [28] rotated by 180°. This instantaneous representation of the flowfield is often associated with the von Kármán vortex street in the far wake of a flow past a bluff body, viewed by an observer who is stationary with respect to the body (see, e.g., Fig. 7 (a) in [28] and Figs. 94–96 in [40]). In our analysis starting in the next section, we take the point of view of an observer moving with the vortices, because only in these coordinates is the background flowfield autonomous.

Because the autonomous system (19)–(20) is periodic in ξ_1 with period $2\pi/\alpha = 2p^* = 7.129$, where $p^* = 3.564$ is the horizontal distance between vortex centers in adjacent rows, values of ξ_1 that differ by an integer multiple of this period can be identified. Thus, the phase space $\mathcal{C}$ of this system can be considered to be the cylinder ξ_1 mod $2p^*$. As pointed out by Andronov, Witt, and Khaikin [1], two different types of periodic orbit are possible on a phase cylinder. A periodic solution of the first kind encircles an equilibrium point on the cylinder, while a periodic solution of the second kind encircles the cylinder itself. As is shown below, attraction by a limit cycle of the second kind plays an important role in our analysis of particle dispersion. Keeping this in mind, for convenience we always unfold the cylinder and depict the phase portraits in the plane. In the next section, we discuss the equations of motion of small particles in the regularized von Kármán vortex street. What we will show is that, for Stokes numbers that are not too large, after an initial transient behavior, the motion of a particle in the assumed background flowfield is controlled by the motion of a corresponding material point in a velocity field that is given by a small dissipative perturbation of the Hamiltonian field in Eqs. (19)–(20). It will be shown in Section V that one effect of this dissipation is to break the respective separatrices that isolate individual vortices and the street from the surrounding flow in the far field.

IV. PARTICLE EQUATIONS OF MOTION

Since Stokes drag is the only force considered here (in addition to inertia), the dimensional equations of motion of a small, rigid, dilute spherical particle in the regularized von Kármán vortex-street flowfield described above are given by

$$\frac{d\boldsymbol{y}}{dt} = \boldsymbol{v}, \tag{21}$$

$$\frac{d\boldsymbol{v}}{dt} = \frac{18\mu}{\rho_p d_p^2}\left[\boldsymbol{u}\left(\boldsymbol{y}, t\right) - \boldsymbol{v}\right], \tag{22}$$

where $\boldsymbol{y} = (y_1,\, y_2)$ denotes the cartesian coordinates of the particle in a reference system that is stationary with respect to the free stream, ρ_p is the particle density, d_p is the particle diameter, μ is the viscosity of the surrounding fluid, $\boldsymbol{v} = (v_1,\, v_2)$ is the particle velocity, and $\boldsymbol{u}(\boldsymbol{y}, t) = (u_1(y_1,\, y_2,\, t),\, u_2(y_1,\, y_2,\, t))$ is the fluid velocity determined by the stream function

ψ_K (Eq. (6)).

In the dimensionless coordinates $\boldsymbol{\xi} = (\xi_1, \xi_2)$ (Eq. (11)) that move at the speed of the vortices relative to the $\boldsymbol{y}$ coordinate system, the particle equations of motion (21)–(22) can be written as an autonomous system of four first-order scalar equations,

$$\frac{d\xi_1}{dt} = \eta_1, \tag{23}$$

$$\frac{d\xi_2}{dt} = \eta_2, \tag{24}$$

$$\frac{d\eta_1}{dt} = \frac{1}{\epsilon}\left[U_K(\xi_1, \xi_2) - \eta_1\right], \tag{25}$$

$$\frac{d\eta_2}{dt} = \frac{1}{\epsilon}\left[V_K(\xi_1, \xi_2) - \eta_2\right]. \tag{26}$$

Here, $U_K(\boldsymbol{\xi})$ and $V_K(\boldsymbol{\xi})$ are defined in (17) and (18), respectively, and the parameter ϵ is a Stokes number defined by

$$\epsilon = \frac{\rho_p d_p^2 c_K}{9\mu b}. \tag{27}$$

Note that the definition of ϵ is based on the vortex street velocity (Eq. (7)) instead of the larger freestream velocity U_∞ employed in the usual definition of Stokes number $\mathbf{St}$ in actual wake flows [37]. Thus,

$$\mathbf{St} = \frac{U_\infty}{c_K}\,\epsilon, \tag{28}$$

so that phenomena that depend on $\mathbf{St}$ will occur at values of ϵ that are smaller than the Stokes numbers in the actual physical systems that we are modeling. In this paper, we are interested in the case when $0 < \epsilon \ll 1$.

Returning to the $\boldsymbol{y}$ coordinate system, nondimensionalized as before, suppose that the initial conditions for a particle are given at time $t = 0$ by

$$\boldsymbol{y}^0 = (y_1^0,\, y_2^0), \qquad \boldsymbol{v}^0 = (v_1^0,\, v_2^0). \tag{29}$$

Then it follows that, in the $\boldsymbol{\xi}$ coordinate system,

$$\boldsymbol{\xi}^0 = (y_1^0,\, y_2^0), \qquad \boldsymbol{\eta}^0 = (v_1^0 - 1,\, v_2^0). \tag{30}$$

Defining a new timescale $\tau = t/\epsilon$ in terms of the small perturbation parameter, the *slow system* (23)–(26) is transformed on the τ time scale into the *fast system* (sometimes called the *inner equations*),

$$\frac{d\xi_1}{d\tau} = \epsilon\,\eta_1, \tag{31}$$
$$\frac{d\xi_2}{d\tau} = \epsilon\,\eta_2, \tag{32}$$
$$\frac{d\eta_1}{d\tau} = U_K(\xi_1, \xi_2) - \eta_1, \tag{33}$$
$$\frac{d\eta_2}{d\tau} = V_K(\xi_1, \xi_2) - \eta_2, \tag{34}$$

which is nonsingular in the limit $\epsilon \to 0$. By Fenichel's geometric singular perturbation theory [11,12] (also see [14,15,29,43]), phase trajectories of the system (23)–(26) are attracted exponentially rapidly to a two-dimensional *center manifold*

$$\begin{aligned} \mathcal{C}_\epsilon = \{(\xi_1, \xi_2, \eta_1, \eta_2) :\ & -\infty < \xi_1 < \infty,\ \ |\xi_2| \le \beta, \\ & \eta_1 = U_K(\xi_1, \xi_2) + h(\xi_1, \xi_2, \epsilon),\ \eta_2 = V_K(\xi_1, \xi_2) + k(\xi_1, \xi_2, \epsilon)\}\,, \end{aligned} \tag{35}$$

i.e., a smooth surface, called the *slow manifold.* This is $2p^*$-periodic in ξ_1, so that it can be interpreted as a cylinder that is a smooth perturbation of $\mathcal{C}$ (with $|\xi_2| \le \beta$). Here, β is a constant that is independent of the Stokes number and sufficiently large to include all points of interest. Furthermore, $\mathcal{C}_\epsilon$ is *locally invariant* in the phase space of the fast system. This means there is a neighborhood $\mathcal{U}$ of $\mathcal{C}_\epsilon$ with the property that the trajectory through each $\boldsymbol{q}$ in $\mathcal{C}_\epsilon$ cannot leave $\mathcal{C}_\epsilon$ without also leaving $\mathcal{U}$, i.e., for as long as the trajectory remains in $\mathcal{U}$ it lies on $\mathcal{C}_\epsilon$. (A trajectory can exit through the boundary of $\mathcal{C}_\epsilon$ in (forward or backward) finite time.) In addition, Fenichel [12] showed that each solution $\boldsymbol{p}(t)$ of (23)–(26) that enters $\mathcal{U}$ is "connected" to a solution $\boldsymbol{q}(t)$ on the slow manifold in the sense that the distance between the two trajectories approaches zero at an exponential rate, as long as the latter solution remains on $\mathcal{C}_\epsilon$.

Substitution of $\mathcal{C}_\epsilon$ into the fast system decouples the first two equations of system (31)–(34) from the latter two,

$$\frac{d\xi_1}{d\tau} = \epsilon \left[U_K(\xi_1, \xi_2) + h(\xi_1, \xi_2, \epsilon)\right], \tag{36}$$
$$\frac{d\xi_2}{d\tau} = \epsilon \left[V_K(\xi_1, \xi_2) + k(\xi_1, \xi_2, \epsilon)\right]. \tag{37}$$

On the slow t time scale, this reduces to a regular perturbation of the streamline equations (19)–(20),

$$\frac{d\xi_1}{dt} = U_K(\xi_1,\, \xi_2) + h(\xi_1, \xi_2, \epsilon), \tag{38}$$
$$\frac{d\xi_2}{dt} = V_K(\xi_1,\, \xi_2) + k(\xi_1, \xi_2, \epsilon). \tag{39}$$

It also follows from Fenichel's theory that the $O(\epsilon)$ terms h and k may be expanded asymptotically in ϵ to any order n,

$$h(\xi_1, \xi_2, \epsilon) = \sum_{j=1}^{n} \epsilon^j h_j(\xi_1, \xi_2) + O(\epsilon^{n+1}), \tag{40}$$
$$k(\xi_1, \xi_2, \epsilon) = \sum_{j=1}^{n} \epsilon^j k_j(\xi_1, \xi_2) + O(\epsilon^{n+1}), \tag{41}$$

with $h_j(\xi_1 + 2p^*, \xi_2) = h_j(\xi_1, \xi_2),\ \ k_j(\xi_1 + 2p^*, \xi_2) = k_j(\xi_1, \xi_2),\ \ j = 1, 2, \ldots, n.$

Coefficients in the expansions (40) and (41) can be computed successively as follows. By local invariance,

$$\frac{d\eta_1}{d\tau} = \frac{\partial U_K}{\partial \xi_1}\frac{d\xi_1}{d\tau} + \frac{\partial U_K}{\partial \xi_2}\frac{d\xi_2}{d\tau} + \frac{\partial h}{\partial \xi_1}\frac{d\xi_1}{d\tau} + \frac{\partial h}{\partial \xi_2}\frac{d\xi_2}{d\tau}. \tag{42}$$

Using (33), (36), (37), (40), (41), and (42),

$$\begin{aligned}
\frac{d\eta_1}{d\tau} &= U_K - \eta_1 = -h = -\epsilon h_1 - \epsilon^2 h_2 - \cdots - \epsilon^n h_n + O(\epsilon^{n+1}) \\
&= \frac{\partial U_K}{\partial \xi_1}\frac{d\xi_1}{d\tau} + \frac{\partial U_K}{\partial \xi_2}\frac{d\xi_2}{d\tau} + \frac{\partial h}{\partial \xi_1}\frac{d\xi_1}{d\tau} + \frac{\partial h}{\partial \xi_2}\frac{d\xi_2}{d\tau} \\
&= \epsilon \left[\frac{\partial U_K}{\partial \xi_1} + \epsilon\frac{\partial h_1}{\partial \xi_1} + \epsilon^2\frac{\partial h_2}{\partial \xi_1} + \cdots + O(\epsilon^{n+1})\right]\left[U_K + \epsilon h_1 + \epsilon^2 h_2 + \cdots + O(\epsilon^{n+1})\right] \\
&+ \epsilon \left[\frac{\partial U_K}{\partial \xi_2} + \epsilon\frac{\partial h_1}{\partial \xi_2} + \epsilon^2\frac{\partial h_2}{\partial \xi_2} + \cdots + O(\epsilon^{n+1})\right]\left[V_K + \epsilon k_1 + \epsilon^2 k_2 + \cdots + O(\epsilon^{n+1})\right].
\end{aligned} \tag{43}$$

Similarly,

$$\frac{d\eta_2}{d\tau} = \frac{\partial V_K}{\partial \xi_1}\frac{d\xi_1}{d\tau} + \frac{\partial V_K}{\partial \xi_2}\frac{d\xi_2}{d\tau} + \frac{\partial k}{\partial \xi_1}\frac{d\xi_1}{d\tau} + \frac{\partial k}{\partial \xi_2}\frac{d\xi_2}{d\tau}. \tag{44}$$

Using (34), (36), (37), (40), (41), and (44),

$$
\begin{aligned}
\frac{d\eta_2}{d\tau} &= V_K - \eta_2 = -k = -\epsilon k_1 - \epsilon^2 k_2 - \cdots - \epsilon^n k_n + O(\epsilon^{n+1}) \\
&= \frac{\partial V_K}{\partial \xi_1}\frac{d\xi_1}{d\tau} + \frac{\partial V_K}{\partial \xi_2}\frac{d\xi_2}{d\tau} + \frac{\partial k}{\partial \xi_1}\frac{d\xi_1}{d\tau} + \frac{\partial k}{\partial \xi_2}\frac{d\xi_2}{d\tau} \\
&= \epsilon \left[\frac{\partial V_K}{\partial \xi_1} + \epsilon \frac{\partial k_1}{\partial \xi_1} + \epsilon^2 \frac{\partial k_2}{\partial \xi_1} + \cdots + O(\epsilon^{n+1})\right] \left[U_K + \epsilon h_1 + \epsilon^2 h_2 + \cdots + O(\epsilon^{n+1})\right] \\
&+ \epsilon \left[\frac{\partial V_K}{\partial \xi_2} + \epsilon \frac{\partial k_1}{\partial \xi_2} + \epsilon^2 \frac{\partial k_2}{\partial \xi_2} + \cdots + O(\epsilon^{n+1})\right] \left[V_K + \epsilon k_1 + \epsilon^2 k_2 + \cdots + O(\epsilon^{n+1})\right]. \qquad (45)
\end{aligned}
$$

Collecting terms of the same order in ϵ, it follows that

$$
\begin{aligned}
h_1 &= -\left[U_K \frac{\partial U_K}{\partial \xi_1} + V_K \frac{\partial U_K}{\partial \xi_2}\right], \qquad (46) \\
h_2 &= -\left[h_1 \frac{\partial U_K}{\partial \xi_1} + k_1 \frac{\partial U_K}{\partial \xi_2} + U_K \frac{\partial h_1}{\partial \xi_1} + V_K \frac{\partial h_1}{\partial \xi_2}\right], \qquad (47) \\
&\cdots \\
h_n &= -\left[h_{n-1} \frac{\partial U_K}{\partial \xi_1} + k_{n-1} \frac{\partial U_K}{\partial \xi_2} + U_K \frac{\partial h_{n-1}}{\partial \xi_1} + V_K \frac{\partial h_{n-1}}{\partial \xi_2}\right. \\
&\quad \left. + \sum_{j=1}^{n-2} h_{n-1-j} \frac{\partial h_j}{\partial \xi_1} + \sum_{j=1}^{n-2} k_{n-1-j} \frac{\partial h_j}{\partial \xi_2}\right], \qquad (48)
\end{aligned}
$$

and

$$
\begin{aligned}
k_1 &= -\left[U_K \frac{\partial V_K}{\partial \xi_1} + V_K \frac{\partial V_K}{\partial \xi_2}\right], \qquad (49) \\
k_2 &= -\left[h_1 \frac{\partial V_K}{\partial \xi_1} + k_1 \frac{\partial V_K}{\partial \xi_2} + U_K \frac{\partial k_1}{\partial \xi_1} + V_K \frac{\partial k_1}{\partial \xi_2}\right], \qquad (50) \\
&\cdots \\
k_n &= -\left[h_{n-1} \frac{\partial V_K}{\partial \xi_1} + k_{n-1} \frac{\partial V_K}{\partial \xi_2} + U_K \frac{\partial k_{n-1}}{\partial \xi_1} + V_K \frac{\partial k_{n-1}}{\partial \xi_2}\right. \\
&\quad \left. + \sum_{j=1}^{n-2} h_{n-1-j} \frac{\partial k_j}{\partial \xi_1} + \sum_{j=1}^{n-2} k_{n-1-j} \frac{\partial k_j}{\partial \xi_2}\right]. \qquad (51)
\end{aligned}
$$

In the next section, we will discuss the qualitative behavior of solutions of the perturbed two-dimensional system (38)–(39).

V. PARTICLE MOTION ON THE SLOW MANIFOLD

In the previous section, we found that, for sufficiently small ϵ, after a rapid initial transient motion toward the slow manifold $\mathcal{C}_\epsilon$, the behavior of particles in the plane wake flow subject to Stokes drag is controlled by the behavior of corresponding material points (we also refer to these as particles in this section) with trajectories on the slow manifold. One immediate conclusion that can be drawn from this fact is that, for $0 < \epsilon \ll 1$, no chaotic dynamics can occur in the system (23)–(26) by application of the Poincaré-Bendixon Theorem (see, e.g., Wiggins [42]). Henceforth, we will restrict our attention to the behavior on $\mathcal{C}_\epsilon$ and study the perturbed system (38)–(39) on the slow manifold for $K = 0.99$. Because we are interested mainly in qualitative features of the trajectories on the slow manifold, we will retain only the first two terms in the perturbation expansion, i.e., set $n = 2$ in (40)–(41), and thus take

$$\frac{d\xi_1}{dt} = U_K(\xi_1,\, \xi_2) + \epsilon h_1(\xi_1, \xi_2) + \epsilon^2 h_2(\xi_1, \xi_2), \tag{52}$$

$$\frac{d\xi_2}{dt} = V_K(\xi_1,\, \xi_2) + \epsilon k_1(\xi_1, \xi_2) + \epsilon^2 k_2(\xi_1, \xi_2), \tag{53}$$

as an approximation to the vector field on the slow manifold. Explicit formulas for the perturbation terms have been obtained using symbolic computation software.

When $\epsilon = 0$, the equations on the slow manifold reduce to the "outer" equations (19)–(20). Representative streamlines of this unperturbed street of Stuart vortices with $K = 0.99$ are shown in Fig. 4. As is clear from the figure, essentially three different types of periodic motion are possible in the unperturbed case. Particles that start inside a separatrix containing a vortex move on a closed periodic orbit of the first kind, in one of two directions. The direction of particle motion is counterclockwise about vortices in the top row and clockwise in the lower row. For particles that start outside the vortex region, motion is on a periodic solution of the second kind to the left, becoming closer to rectilinear the further away it gets from the vortex street. The most interesting periodic behavior from the point of view of particle focusing, however, occurs for particles that are located in the jet that undulates through the vortices. This is because it is this type of periodic motion of the second kind that we employ in order to explain the particle-focusing behavior that has been observed both in laboratory experiments [37] and in numerical simulations of these experiments [37,6] (see Fig. 1). The question we address in what follows is, how does the $\epsilon = 0$ phase portrait given in Fig. 4 perturb for $0 < \epsilon \ll 1$? Our approach to this problem is to study the qualitative behavior of trajectories of the approximate system of equations (52)–(53) using numerical methods. We will show that for sufficiently small values of ϵ, there is an attracting limit cycle of the second kind in the region of the central jet. As we will demonstrate, this non-fractal attractor provides a mechanism for the focusing phenomenon observed by Tang, et al. [37].

It is easy to verify that the equilibrium points of the vector field on the slow manifold are at the same locations as those for the unperturbed vortex street. In particular, for the chosen vortex spacing (Eq. (9)), there is a saddle point at $(\xi_1, \xi_2) = (p^*, q^*) = (3.564, 2.052)$ and a vortex center at $(p^*, -1.000)$; locations of the other equilibrium points can be found from these two. It is also straightforward to check that the saddle points in the unperturbed flow remain saddle points in the perturbed motion. However, the vortex center points that are neutrally stable in the unperturbed motion become unstable under the influence of the perturbations introduced by particle inertia (i.e., centrifugal effects). This can be shown by linearizing the vector field about a vortex center point. Thus, under the perturbation induced by particle inertia, the vortex centers become spiral sources, so that the qualitative behavior of the phase trajectories changes significantly under the influence of Stokes drag.

The perturbed equations (52)–(53) were checked by verifying that particle trajectories for values of ϵ between 0.001 and 0.25 as computed by numerical integrations (utilizing the ODE solver package DEPAC [30]) of this approximate system agreed closely with solutions of the original system Eqs. (23)–(26). Initial particle velocities for the latter system were taken as the vortex street velocity, i.e., a particle was initially stationary in the $\boldsymbol{\xi}$-$\boldsymbol{\eta}$ phase space. We found that, after an initial transient deviation for larger ϵ due to the fact that particles in the original system did not start exactly on the center manifold $\mathcal{C}_\epsilon$, corresponding curves of particle position vs. time for the two solutions virtually overlay, indicating that the approximate perturbation solution with $n = 2$ does, in fact, apply here over the indicated range of the small parameter.

Several computer simulations were carried out in order to gain an understanding of how the qualitative behavior of the system (52)–(53) depends on ϵ. All of these calculations were performed utilizing DEPAC. Fig. 8 shows the results of numerical simulations of Eqs. (52)–(53) with $\epsilon = 0.05,\ 0.15$, and 0.25, with the same three initial values in each case, $(\xi_1, \xi_2) = (0.000,\ 2.000)$, $(0.500 - p^*,\ -1.000)$, $(-0.200 - 2p^*,\ 1.000)$. As can be seen in the figure, all three orbits spiral outward from the vortex center for each value of the ϵ. In (a), a pair of orbits asymptotically approaches a periodic attractor in the system, while the third orbit exits the region of the vortex street. In Fig. 8(b), a different pair of orbits approaches a periodic attractor more rapidly than in (a) while the third exits the street region. In the terminology of Andronov, Witt, and Khaikin [1], in these first two cases there is an asymptotically stable limit cycle of the second kind in the motion on the invariant manifold $\mathcal{C}_\epsilon$. Finally, in (c), all three orbits exit the vortex region and there is no longer an attractor in this region.

Fig. 9 indicates how the qualitative behavior of the perturbed system evolves with increasing ϵ. The figure was made by computing the two incoming and two outgoing "whiskers", i.e., the "halves" of the stable and unstable manifolds, respectively, of the saddle point $(-p^*, q^*)$ (see, e.g., [42] for definitions), for $\epsilon = 0.05,\ 0.15,\ 0.24$, and 0.25. It is clear that an important effect of the dissipation in the system is to break the homoclinic and heteroclinic separatrices that, respectively, isolate individual vortices and connect adjacent saddle points in the unperturbed vortex street (see Fig. 4). Note that, in all but the last case, the two stable whiskers originate at a vortex center in the lower row of the street. The last plot indicates that the qualitative behavior of the stable and unstable manifolds of the saddle points on the slow manifold undergoes a bifurcation at a critical value of ϵ in the interval $0.24 < \epsilon < 0.25$ such that, for larger values of ϵ, the incoming whisker to the saddle point originates in the adjacent vortex on the upper row rather than at a vortex point on the lower row. This set of calculations was done by starting at the saddle point and integrating the appropriate equation $d\xi_1/d\xi_2$ or $d\xi_2/d\xi_1$ for the trajectory, with the singularity in the vector field at the saddle point removed by an application of L'Hospital's rule. Once the local invariant manifold was approximated, its endpoint was used as initial data for equations (52)–(53), which were integrated either forward or backward in time, as appropriate. In the case of the incoming whiskers of the saddle point that originate at vortex centers, calculations were performed backwards in time and were terminated when the trajectories arrived in a small neighborhood of the vortex center in order to avoid excessive run times. This is why these two orbits do not always appear to meet at a vortex center in the set of figures we discuss next.

In Figs. 10–13 the same kind of data for $\epsilon = 0.015,\ 0.05,\ 0.15$, and 0.25 has been plotted by rotating and translating the invariant manifolds of a single saddle point using the identities $U_K(\xi_1 + p^*, -\xi_2) + h(\xi_1 + p^*, -\xi_2) = U_K(\xi_1, \xi_2) + h(\xi_1, \xi_2)$ and $V_K(\xi_1 + p^*, -\xi_2) + k(\xi_1 + p^*, -\xi_2) = -V_K(\xi_1, \xi_2) - k(\xi_1, \xi_2)$. These figures give a good idea of how the *domain of attraction* of the limit cycle, i.e., the set of points $\boldsymbol{q}$ in $\mathcal{C}_\epsilon$ that approach the limit cycle as $t \to \infty$, changes with increasing ϵ. The cases $\epsilon = 0.015$ (Fig. 10) and $\epsilon = 0.05$ (Fig. 11) show how increasingly intertwined this domain of attraction, which could be called the *capture set*, and its complement, which could be called the *escape set*, become as ϵ decreases. In both figures, the capture set corresponds to points starting outside the narrow spiral region originating at the vortex center. This suggests, but certainly does not prove, that as $\epsilon \to 0$ there is a type of sensitive dependence on initial conditions (see e.g., Arnold [4], Neishtadt [25]) in the nonchaotic dynamical system (38)–(39). Also note that, in the case of $\epsilon = 0.05$ (Fig. 11), particle focusing, i.e., close approach to the limit cycle, has already begun to occur by the time a particle has advanced down the street by a single period $2p^*$. This focusing is much more pronounced after a single period in the case $\epsilon = 0.15$ (Fig. 12). Also notice that the central jet narrows rapidly with increasing ϵ, thus enhancing the focusing effect. By the time that ϵ has increased to 0.25 (Fig. 13), a bifurcation in the qualitative behavior of the saddle point separatrices of the motion on the slow manifold has taken place. Thus, since there is no longer an attractor in the system, no focusing can occur although, as is evident from the figure, particles escape from the vortex region along very narrow channels formed by the separatrices. Eventually, ϵ will become too large for the results of the singular perturbation theory to apply.

A simple complementary explanation of the focusing phenomenon can also be given based on centrifugal force considerations. In Figs. 14 and 15, particle spin-out times from a vortex center have been computed and plotted, utilizing Eqs. (23)–(26), for various values of ϵ in the interval $0.01 < \epsilon < 0.50$. The numerical integrations were carried out by means of a simple method [24] whereby the particle equations are integrated exactly from one time step to the next assuming constant flow velocity, a scheme that gives results virtually identical to DEPAC but is easier to use. Particles were inserted with zero velocity at the indicated vortex center in the upper row, and the spin-out times it took for them to reach a circle (see Fig. 14) with radius equal to half the distance between the initial position and the closest vortex centers in the lower row were calculated. The trajectories are shown in Fig. 14, while Fig. 15 is a plot of the spin-out times as a function of ϵ. These times have been normalized with respect to the time it would take for a vertical reference line in the fluid flow that is traveling in the street direction but faster to move a distance equal to one horizontal vortex spacing $p^* = 3.564$. This is analogous to a characteristic passage time for the downstream movement of vortices as they are shed from the rear of a bluff body, as will become clear in later figures. For the results presented in Fig. 15, the reference line is moving at four times the street velocity, a factor that has no essential effect on the nature of the results. The symbols in the figure represent the particle spin-out times while the solid line is a curve fit with inverse dependence on ϵ, since the radial force depends linearly on mass (i.e., ϵ). As can be seen, the normalized spin-out times, T_s, increase to much greater than one as ϵ becomes much less than approximately 0.10. Thus, particles in this size range do not spin out to the vortex peripheries until they are far downstream of the reference line, i.e., bluff body. Therefore, although particle focusing could in principle eventually occur, in most realistic flows this would be too far downstream for the wake to remain coherent. For

$\epsilon \gtrsim 0.15$, the spin-out times become close to unity, and thus focusing occurs early in the far-wake region. This corresponds to the focusing at Stokes numbers near one that has been previously reported [6,37]. For $\epsilon \gg 1$, however, particle inertial effects are more important and dispersion occurs too rapidly for focusing to occur, as can be seen from the bottom frame ($\mathbf{St} = 10.0$) in Fig. 1. For very large Stokes number (i.e., order 100), dispersion becomes negligible once again as particles are simply convected downstream with little lateral motion [6,37]. Note that the above physical description of the focusing process is entirely consistent with the analysis of Druzhinin [9] in which Stokes number-dependent particle concentration waves evolve in an axisymmetric vortex on a ϵ^{-1} time scale.

Figs. 16 and 17 are streakline plots in which a vertical reference line of length two representing the rear face of a bluff body is moving at four times the street velocity to the right while ejecting particles at zero velocity (approximately corresponding to the particle injection conditions in Fig. 1) in the moving frame. Note that this correctly simulates the circulation pattern of vortices being shed alternately from the top and the bottom of a bluff body moving with the street, but faster, in the $+\xi_1$-direction. The Strouhal number (nondimensional frequency based on reference line length and velocity relative to the street) of this shedding (two vortices shed) is independent of line velocity and is simply the vortex spacing ratio $b/a = 0.281$ for line length $b = 2$. This is approximately twice the value (based on free-stream velocity) typically observed for laminar shedding from square cylinders [7,8]. Finally it is noted that the definition of Stokes number $\mathbf{St}$ based on line velocity relative to the street would be triple the value of ϵ employed here.

The solid line in Figs. 16 and 17 represents the limit cycle of the perturbation solution and is thus the envelope (i.e., attractor) toward which particles should spiral asymptotically as they move downstream through the vortex street. These figures are thus intended to be reasonably analogous to the visualizations of the full Navier-Stokes simulations depicted in Fig. 1. As can be seen, the particles with $\epsilon = 0.01$ in Fig. 16 do not spin out to the limit cycle in the region of the far wake shown here. At the larger ϵ of 0.20 in Fig. 17, spin-out times are much smaller and focusing is clearly seen as the particles now concentrate in a thin region about the limit cycle. This demonstrates conclusively that the focusing phenomenon observed in previous numerical and experimental investigations [6,37] does in fact also occur in this simplified model problem for appropriate values of ϵ. Fig. 18 visualizes an extended wake region of the far wake for $\epsilon = 0.015$ in order to illustrate that the particles eventually do spin out to the attracting limit cycle even at very small Stokes numbers.

VI. CONCLUDING REMARKS

To summarize, we have presented a perturbation study of the dynamics of small particles subject to Stokes drag in the wake of a bluff body. The motivation for the problem addressed here has been the interesting phenomenon of "particle focusing". Tang, et al. [37] observed that over a range of Reynolds numbers, dilute particles injected in the flow behind a bluff body tend not to mix, as might be expected, but rather to concentrate in narrow bands on the outer boundaries of the vortices in the street that forms in the far wake. Based on our analysis, we have argued that the presence of a periodic attractor in a simplified approximation of the dynamics of dilute particles in the far wake provides a plausible mechanism for the observed organized particle dynamics. This periodic attractor corresponds to a unique one-dimensional curve in the "instantaneous alleyway" that Perry, Chong, and Lim [28] have shown exists in the flow downstream from the bluff body. The analysis that we have presented makes it clear that the attractor is present because of dissipative effects due to particle motion. Thus, in the limiting case $\epsilon = 0$ where there is no Stokes drag, particles simply track the background flowfield, and no attractor is present in the dynamical system for the particles.

In order to formulate our simplified particle dynamics model, we have replaced the background flowfield in the far wake with respect to an observer moving with the vortices by a spatially-periodic von Kármán vortex street, modified by Stuart's regularization of the singularities at the point-vortex centers. We have argued that, for Reynolds numbers on the order of 100, this is a reasonable approximation over a portion of the far wake downstream from a bluff body that includes at least several vortices. Using ϵ as a small parameter, where ϵ is the Stokes number defined by the street velocity rather than the larger Stokes number **St** defined with respect to the free stream velocity, we have applied Fenichel's geometric singular perturbation theory to study the dynamics of particles for which ϵ is not too large. We have shown that, after an initial transient behavior, the motion in four-dimensional position-velocity phase space of a dilute particle is controlled by the motion of a material point on a two-dimensional center manifold that can be identified with a cylinder. On this reduced-dimension center manifold, the vector field that controls the particle motion is a dissipative $O(\epsilon)$ perturbation of the Hamiltonian vector field determined by the stream function of the regularized vortex street. By analyzing the behavior of material points in the two-dimensional perturbed system numerically, we have elucidated qualitative features (e.g., Figs. 8–17) of particle motion in the original four-dimensional system that would have been difficult to establish by numerical methods alone.

In particular, we have shown that, for ϵ not too large, two important effects of the dissipation are to change the neutrally stable vortices into unstable sources, and to break the respective separatrices that isolate the individual vortices in the unperturbed regularized vortex street from each other and from the free stream. For ϵ less than approximately 0.25, we have shown that, as a result of these dissipative effects, there is a unique limit-cycle attractor in the region of the jet that undulates over and under adjacent vortices in the unperturbed street, and we have computed the spiral structure of its domain of attraction. Furthermore, we have established that there is a particle spin-out time scale inversely proportional to ϵ, and a rate of attraction of particles toward the limit cycle that is directly proportional to ϵ. As a result, we have shown that focusing is most likely to be observed in a given wake flow for ϵ near 0.25, which typically corresponds to a Stokes number of the order of one in a two-dimensional flow past a bluff body. Thus, our analysis provides a plausible explanation for the "particle-focusing" phenomenon that has been observed in both laboratory experiments and numerical simulations [6,37]. Because the essential dynamics takes place on a two-dimensional phase space, the focusing mechanism we have proposed has nothing to do with chaotic dynamics. Finally, since small particles are often used to visualize wake flows, this study of the effects of Stokes drag on the dynamics of small particles in wakes could also have implications for flow visualization studies.

ACKNOWLEDGMENTS

It is a pleasure to thank C. K. R. T. Jones for helpful conversations and for providing us with a copy of Haffner's unpublished paper [14]. We would also like to acknowledge the helpful comments of some anonymous referees.

REFERENCES

[1] A. A. Andronov, A. A. Witt, and S. E. Khaikin, *Theory of Oscillators* (Pergamon Press, New York, 1966).

[2] H. Aref, "Integrable chaotic and turbulent vortex motion in two-dimensional flows," Ann. Rev. Fluid Mech. **13**, 345-389 (1983).

[3] H. Aref and N. Pomphrey, "Integrable and chaotic motion of four vortices. I. The case of identical vortices," Proc. Roy. Soc. London **A380**, 359-387 (1982).

[4] V. I. Arnold, "Small denominators and problems of stability of motion in classical and celestial mechanics," Usp. Mat. Nauk **18**, 91-192 (1963) [English Translation: Russian Math. Surveys **18**, 85-191 (1963)].

[5] C. T. Crowe, T. R. Troutt, and J. N. Chung, "Numerical models for two-phase turbulent flows," Ann. Rev. Fluid Mech. **28**, 11-43 (1996).

[6] C. T. Crowe, T. R. Troutt, J. N. Chung, R. W. Davis, and E. F. Moore, "A turbulent flow without particle mixing," Aerosol Science and Technology **22**, 135-138 (1995).

[7] R. W. Davis and E. F. Moore, "A numerical study of vortex shedding from rectangles," J. Fluid Mech. **116**, 475-506 (1982).

[8] R. W. Davis, E. F. Moore, and L. P. Purtell, "A numerical-experimental study of confined flow around rectangular cylinders," Phys. Fluids **27**, 46-59 (1984).

[9] O. A. Druzhinin, "Concentration waves and flow modification in a particle-laden circular vortex," Phys. Fluids **6**, 3276-3284 (1994).

[10] J. Duan and S. Wiggins, "Lagrangian transport and chaos in the near wake of a cylinder in the time-periodic regime: a numerical implementation of lobe dynamics," Nonlinear Processes in Geophysics **4**, 125-136 (1997).

[11] N. Fenichel, "Persistence and smoothness of invariant manifolds for flows," Indiana

Univ. Math. J. **21**, 193-226 (1971).

[12] N. Fenichel, "Geometric singular perturbation theory for ordinary differential equations," J. Differential Equations **31**, 51-98 (1979).

[13] P. Grassberger and I. Procaccia, "Measuring the strangeness of strange attractors," Physica D **9**, 189-208 (1983).

[14] T. Haffner, "Dynamik von Teilchen in einer periodische Wirbelströmung," Diplomarbeit, Department of Mathematics, University of Stuttgart, September 1995.

[15] C. K. R. T. Jones, "Geometric singular perturbation theory," in *Springer Lecture Notes in Mathematics* **Vol. 1609**, edited by R. Johnson, Springer-Verlag, New York, 1995, pp. 44-120.

[16] H. Lamb,*Hydrodynamics*, 6th Edn., Cambridge University Press, Cambridge, UK, 1993.

[17] B. Marcu and E. Meiburg, "The effect of streamwise braid vortices on the particle dispersion in a plane mixing layer. I. Equilibrium points and their stability," Phys. Fluids **8**, 715-733 (1996).

[18] B. Marcu, E. Meiburg, and P. K. Newton, "Dynamics of heavy particles in a Burgers vortex," Phys. Fluids **7**, 400-410 (1995).

[19] B. Marcu, E. Meiburg, and N. Raju, "The effect of streamwise braid vortices on the particle dispersion in a plane mixing layer. II. Nonlinear particle dynamics," Phys. Fluids **8**, 734-753 (1996).

[20] J. E. Martin and E. Meiburg, "The accumulation and dispersion of heavy particles in forced two-dimensional mixing layers. I. The fundamental and subharmonic cases," Phys. Fluids **6**, 1116-1132 (1994).

[21] M. R. Maxey and J. J. Riley, "Equation of motion for a small rigid sphere in a nonuniform flow," Phys. Fluids **26**, 883-889 (1983).

[22] E. Meiburg and P. K. Newton, "Particle dynamics and mixing in a viscously decaying shear layer," J. Fluid Mech. **227**, 211-244 (1991).

[23] L. M. Milne-Thomson, *Theoretical Hydrodynamics*, 5th ed. (Macmillan, London, UK, 1968).

[24] E. F. Moore and R. W. Davis, "Numerical computation of particle trajectories: a model problem," *Gas-Solid Flows–1986*, ASME Pub. FED–Vol. 35, American Society of Mechanical Engineers, New York, NY, pp. 111-116 (1986).

[25] A. I. Neishtadt, "Probability phenomena due to separatrix crossing," CHAOS **1**, 42-48 (1991).

[26] E. Ott and T. Tél, "Chaotic scattering: an introduction," CHAOS **3**, 417-437 (1994).

[27] J. M. Ottino, *The Kinematics of Mixing: Stretching, Chaos, and Transport* (Cambridge University Press, Cambridge, UK, 1989).

[28] A. E. Perry, M. S. Chong, and T. T. Lim, "The vortex-shedding process behind two-dimensional bluff bodies," J. Fluid Mech. **116**, 77-90 (1982).

[29] J. Rubin, C. K. R. T. Jones, and M. Maxey, "Settling and asymptotic motion of aerosol particles in a cellular flow field," J. Nonlinear Sci. **5**, 337-358 (1995).

[30] L. F. Shampine and H. A. Watts, "DEPAC - Design of a user oriented package of ODE solvers," SAND79-2374, Sandia National Laboratories, Albuquerque, NM, 1979.

[31] P. G. Saffman, *Vortex Dynamics* (Cambridge University Press, Cambridge, UK, 1995).

[32] P. G. Saffman and J. C. Schatzman, "Properties of a vortex street of finite vortices," SIAM J. Sci. Stat. Comput. **2**, 285-295 (1981).

[33] K. Shariff, T. H. Pulliam, and J. M. Ottino, "A dynamical systems analysis of kinematics in the time-periodic wake of a circular cylinder," Lectures in Applied Mathematics **28**, 613-646 (1991).

[34] J. C. Sommerer, H.-C. Ku, and H. E. Gilreath, "Experimental evidence for chaotic scattering in a fluid wake," Phys. Rev. Letters **77**, 5055-5058 (1996).

[35] J. C. Sommerer, E. Ott, and T. Tél, "Modeling two-dimensional fluid flows with chaos theory," Johns Hopkins APL Technical Digest **18**, 193-203 (1997).

[36] J. T. Stuart, "On finite amplitude oscillations in laminar mixing layers," J. Fluid Mech. **29**, 417-440 (1967).

[37] L. Tang, F. Wen, Y. Yang, C. T. Crowe, J. N. Chung, and T. R. Troutt, "Self-organizing particle dispersion mechanism in a plane wake," Phys. Fluids A **4**, 2244-2251 (1992).

[38] K.-K. Tio, A. M. Ganán-Calvo, and J. C. Lasheras, "The dynamics of small, heavy, rigid spherical particles in a periodic Stuart vortex flow," Phys. Fluids A **5**, 1679-1693 (1993).

[39] K.-K. Tio, A. Liñán, J. C. Lasheras, and A. M. Ganán-Calvo, "On the dynamics of buoyant and heavy particles in a periodic Stuart vortex flow," J. Fluid Mech. **254**, 671-699 (1993).

[40] M. Van Dyke, *An Album of Fluid Motion*, Parabolic Press, Stanford, CA, 1982.

[41] F. Wen, N. Kamalu, J. N. Chung, C. T. Crowe, and T. R. Troutt,"Particle dispersion by vortex structures in plane mixing layers," ASME J. Fluid Engineering **114**, 657-666 (1992).

[42] S. Wiggins, *Introduction to Applied Nonlinear Dynamical Systems and Chaos* (Springer-Verlag, New York, 1990).

[43] S. Wiggins, *Normally Hyperbolic Invariant Manifolds in Dynamical Systems* (Springer-Verlag, New York, 1994).

FIGURES

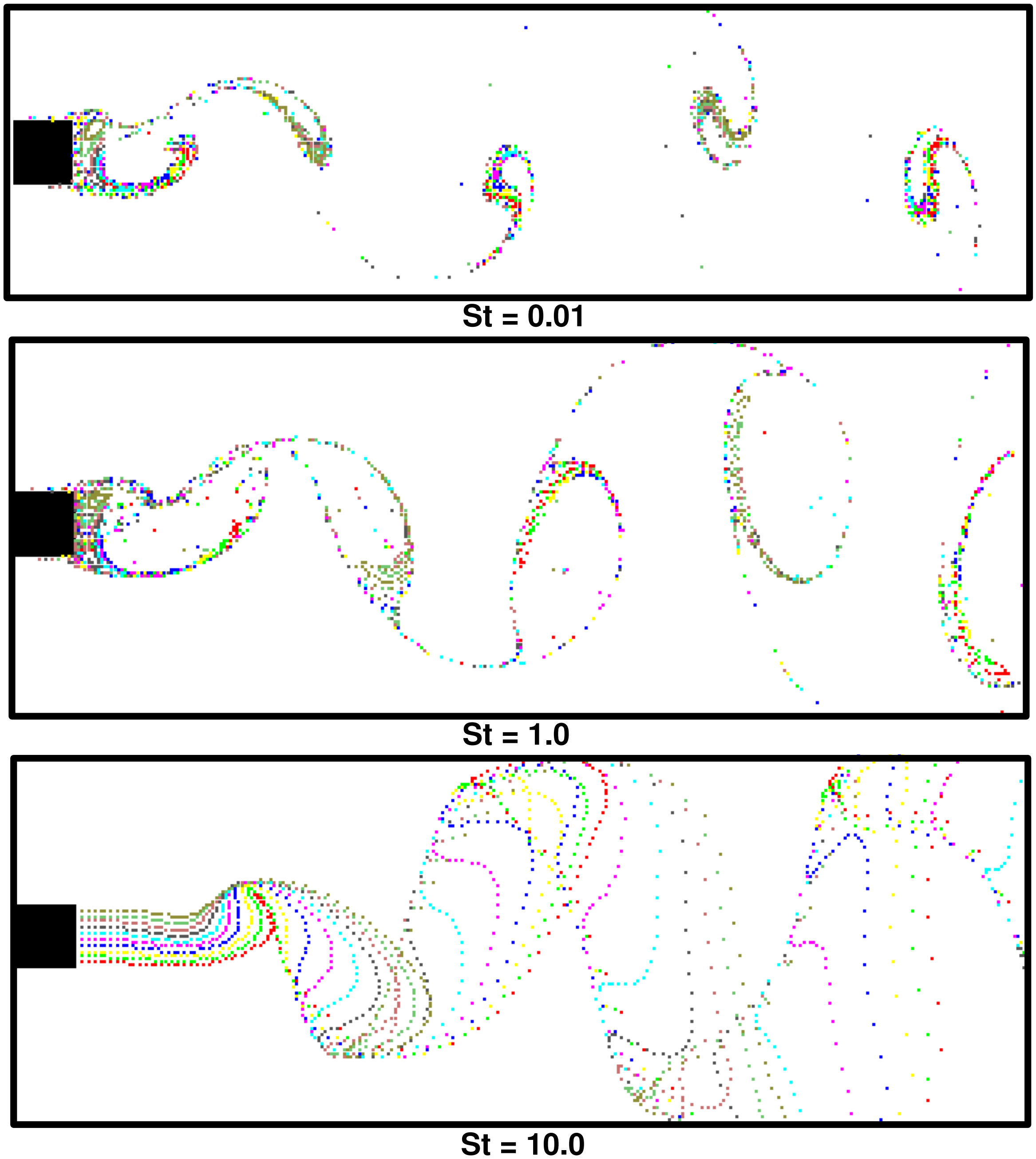

FIG. 1. Three numerical simulations of a two-dimensional laminar fluid flow around a square cylinder illustrate the "particle-focusing" phenomenon that occurs here at $\mathbf{St} = 1$.

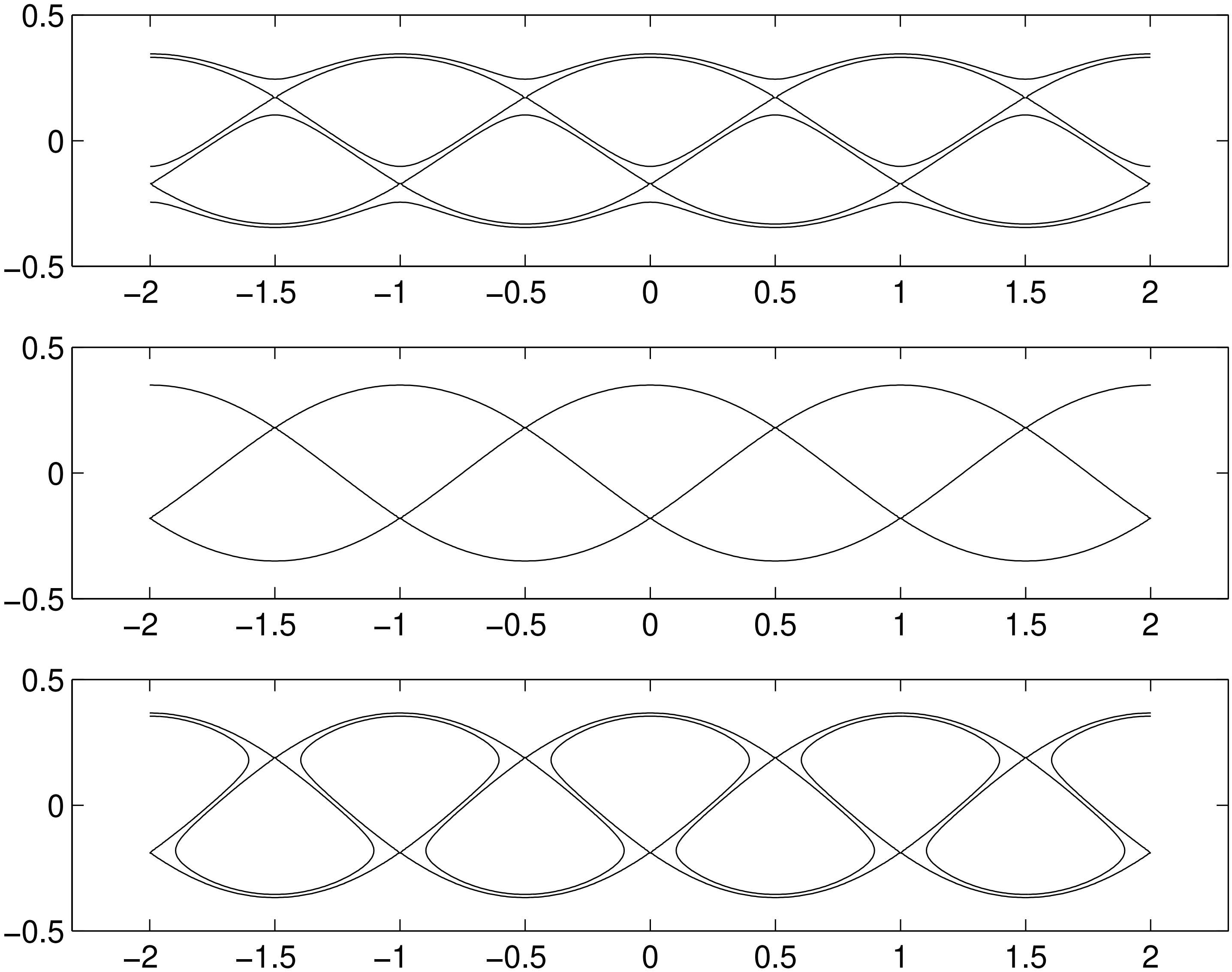

FIG. 2. Level curves of Ψ_K that pass through the saddle equilibrium points for $K = 0.25$, 0.2991, and 0.35.

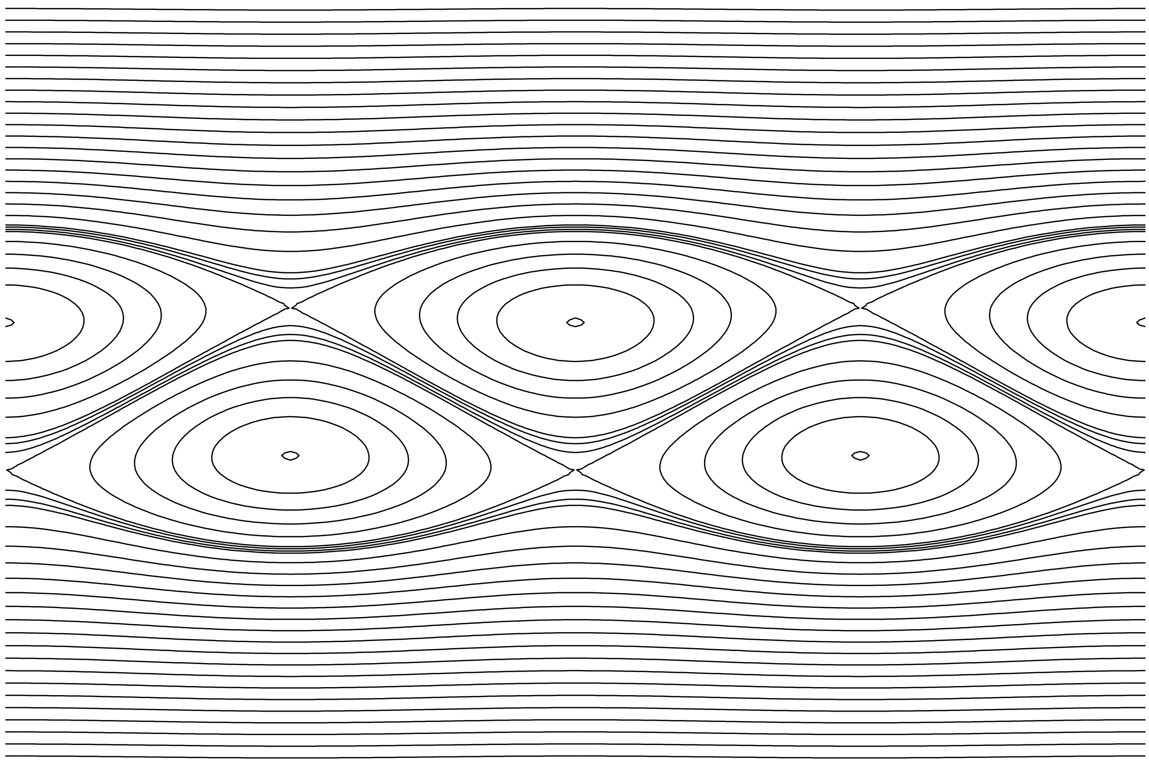

FIG. 3. Streamlines of the regularized von Kármán street from the point of view of an observer moving with the vortices for $K = 0.25$. Upper row of "Kelvin cat eyes" consists of vortices rotating in a counterclockwise sense, while those in the lower row rotate clockwise. Flow outside the vortex region is to the left, while a jet between the rows moves to the right.

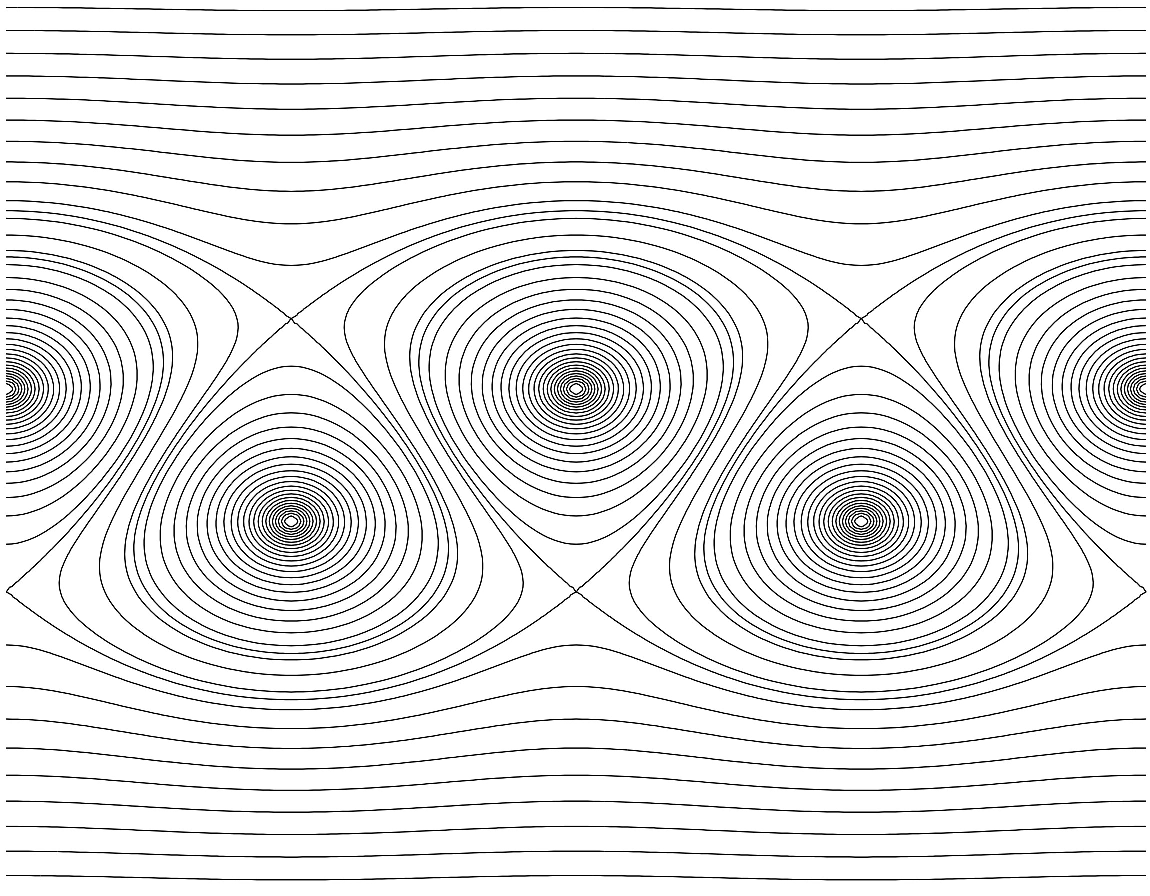

FIG. 4. Streamlines of the regularized von Kármán street ($K = 0.99$) from the point of view of an observer moving with the vortices. Each vortex is now isolated from the others by a single separatrix. The free stream moves to the left at a (dimensionless) speed of one, while the jet in the central region now also moves to the left.

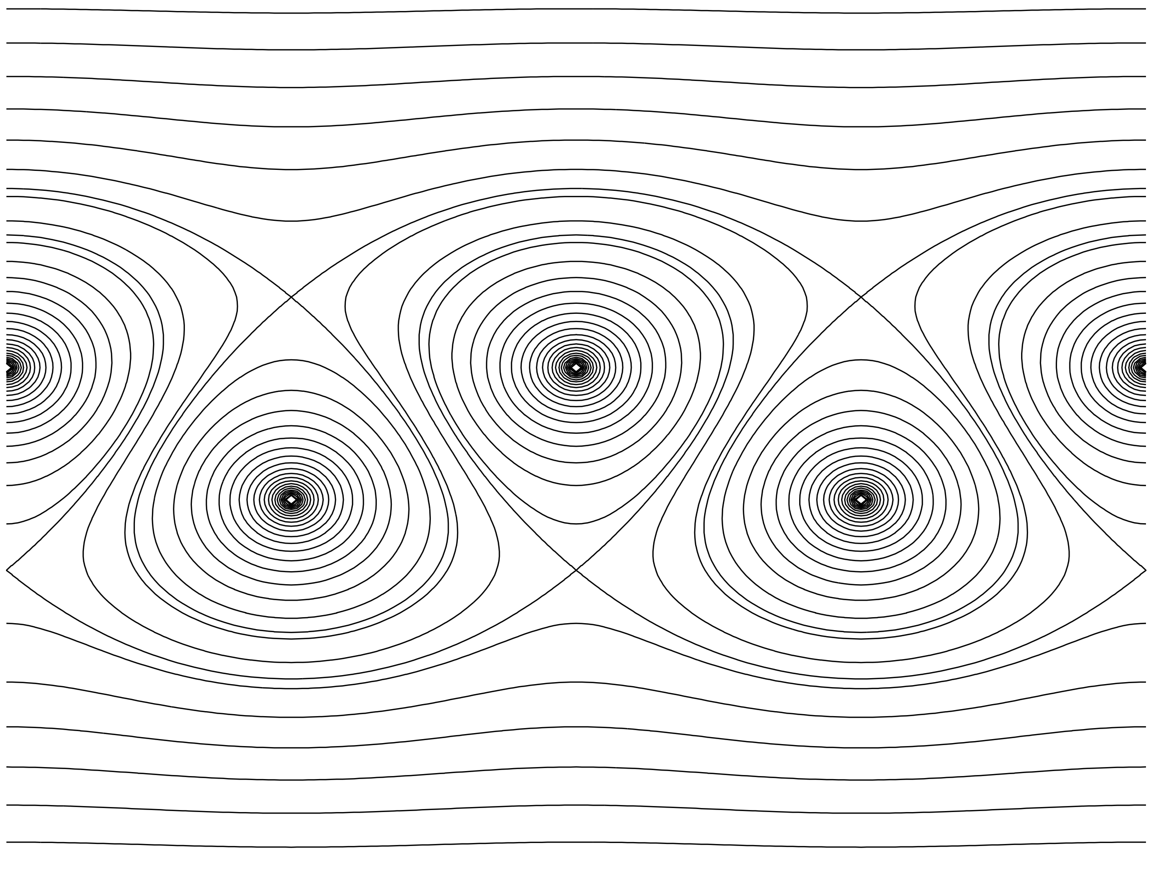

FIG. 5. Streamlines of the unmodified von Kármán street ($K = 1$) from the point of view of an observer moving with the vortices. Note the close similarity to the case $K = 0.99$ in the previous figure.

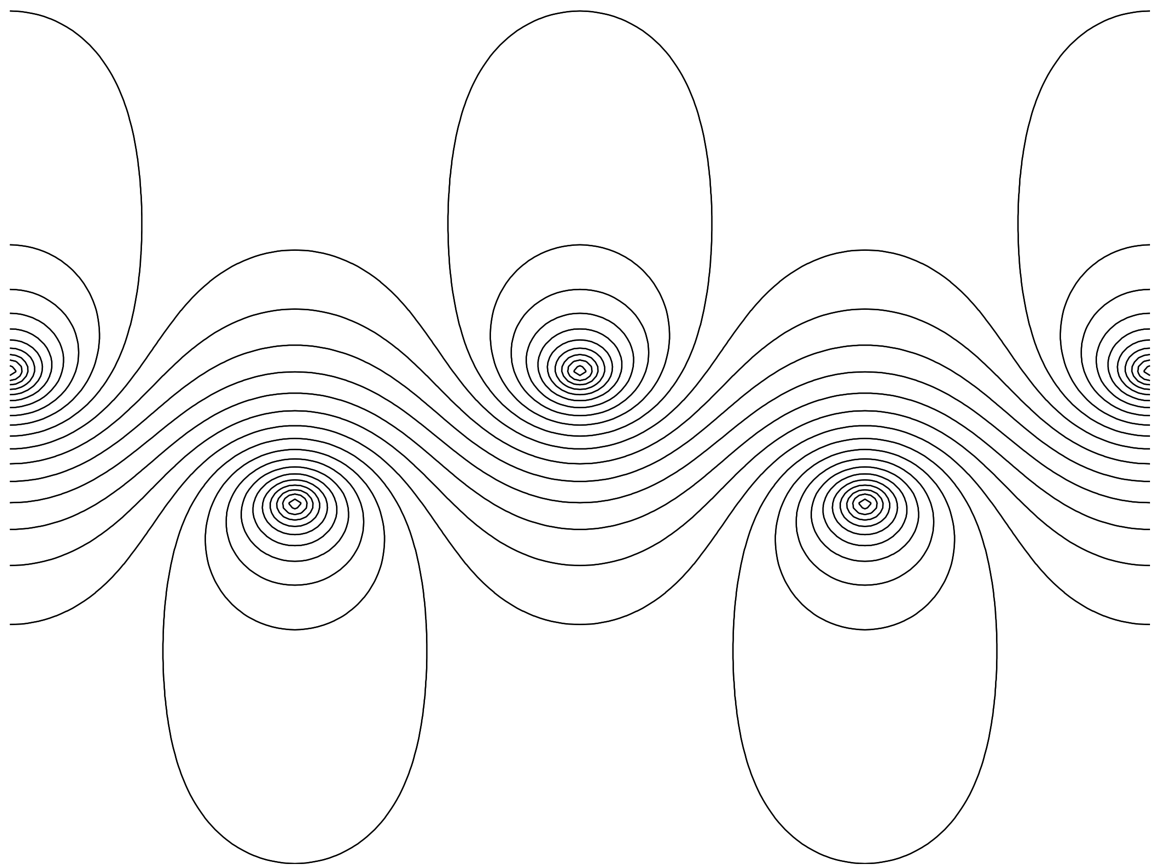

FIG. 6. Streamlines at $t = 0$ of the regularized von Kármán street ($K = 0.99$) from the point of view of an observer moving with the free stream. The street is moving to the right at a (dimensionless) speed of one.

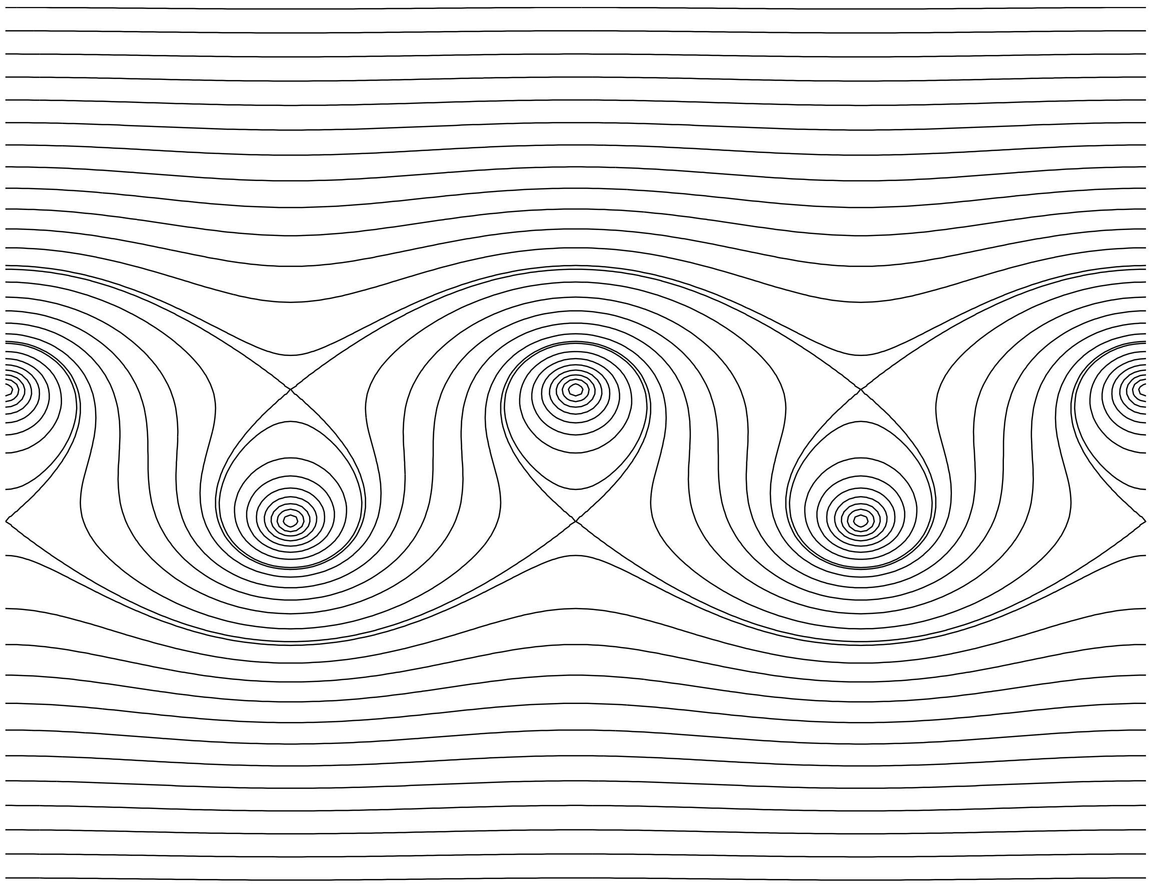

FIG. 7. Streamlines at $t = 0$ of the regularized von Kármán street ($K = 0.99$) from the point of view of an observer moving slower than both the free stream and the street. The street is moving to the left at a speed of one, and the free stream is moving to the left at a speed of two.

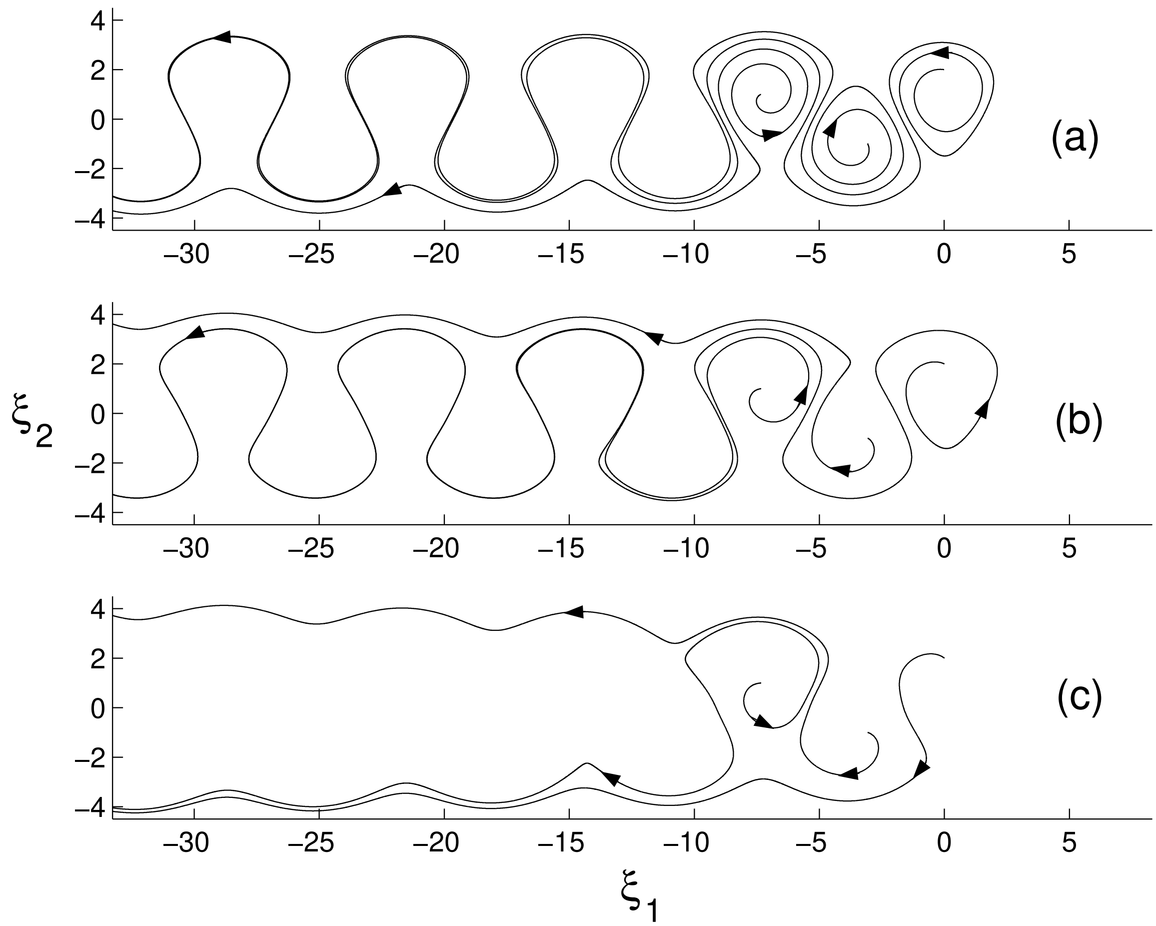

FIG. 8. Orbits corresponding to three different sets of initial conditions, $(\xi_1, \xi_2) = (0.0,\ 2.0)$, $(0.5 - p^*,\ -1.0)$, $(-0.2 - 2p^*,\ 1.0)$, with (a) $\epsilon = 0.05$, (b) $\epsilon = 0.15$, and (c) $\epsilon = 0.25$. In (a), two orbits asymptotically approach a limit cycle of the second kind, while the third orbit exits the region of the vortex street; in (b), a different pair of orbits approaches a limit cycle of the second kind, while the other orbit exits the street region; in (c), all orbits exit the vortex region.

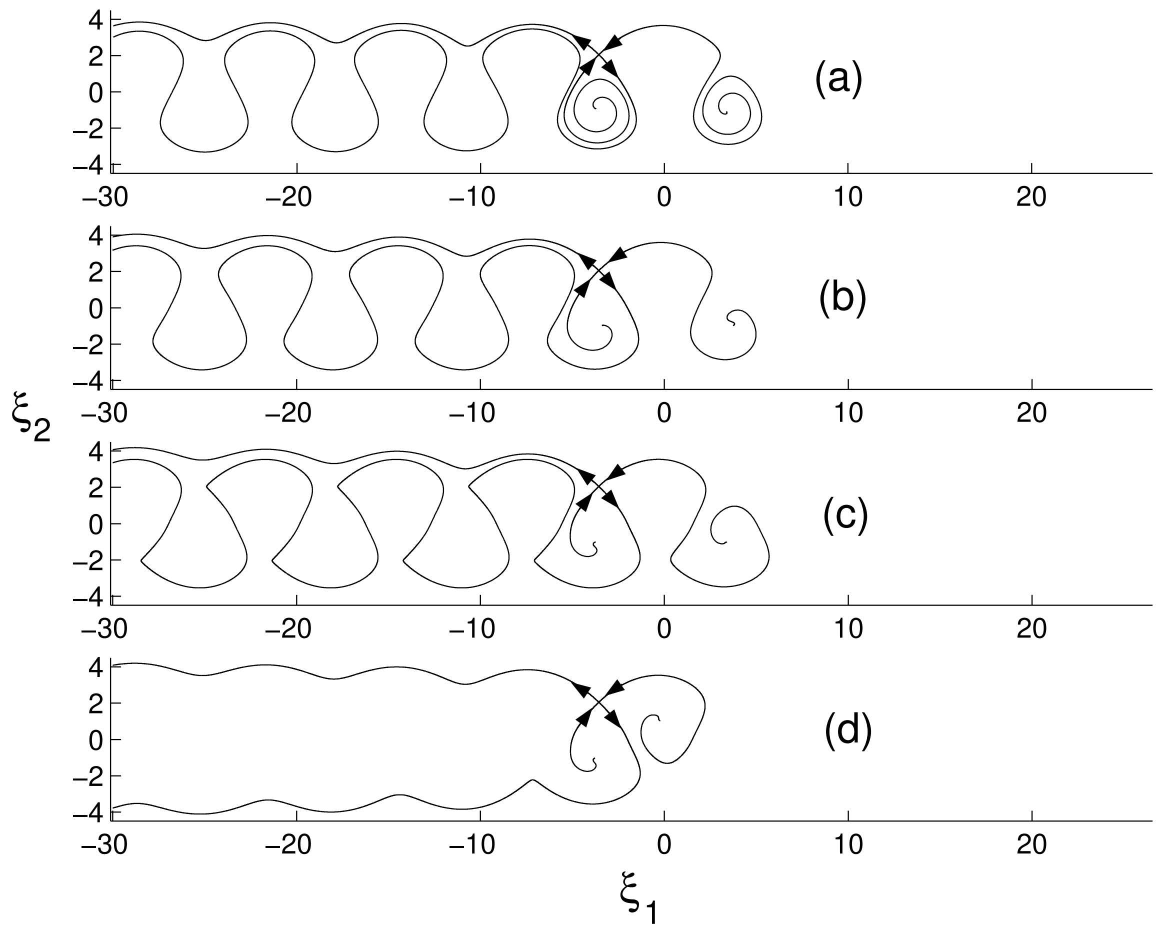

FIG. 9. Incoming and outgoing "whiskers" of the saddle point located at $(-p^*, q^*)$ in the perturbed motion, with (a) $\epsilon = 0.05$, (b) $\epsilon = 0.15$, (c) $\epsilon = 0.24$ and (d) $\epsilon = 0.25$. Dissipatation causes the saddle-to-saddle connecting orbits in the unperturbed flow to break. Also, for some critical value of ϵ between the last two cases, a bifurcation in the qualitative behavior of the particle dynamics takes place.

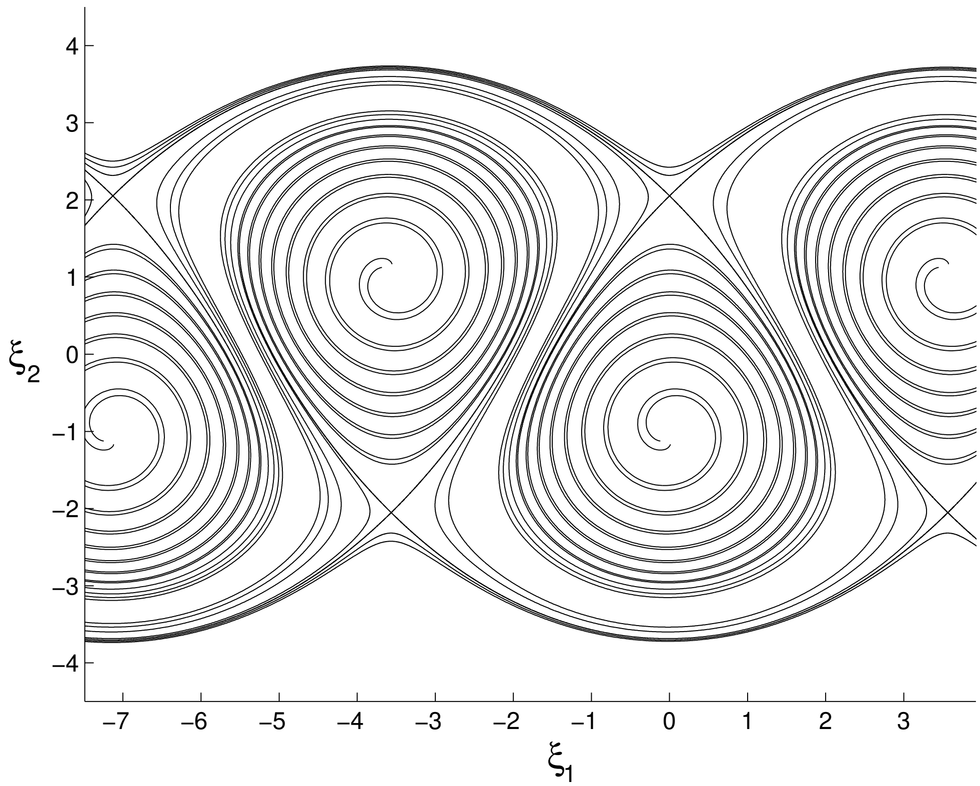

FIG. 10. Incoming and outgoing "whiskers" of several adjacent saddle points in the perturbed motion, with $\epsilon = 0.015$, show the complexity of the domain of attraction of the limit cycle for very small ϵ. Particles starting outside the narrow spiral asymptotically approach the limit cycle, whereas those inside the narrow spiral escape.

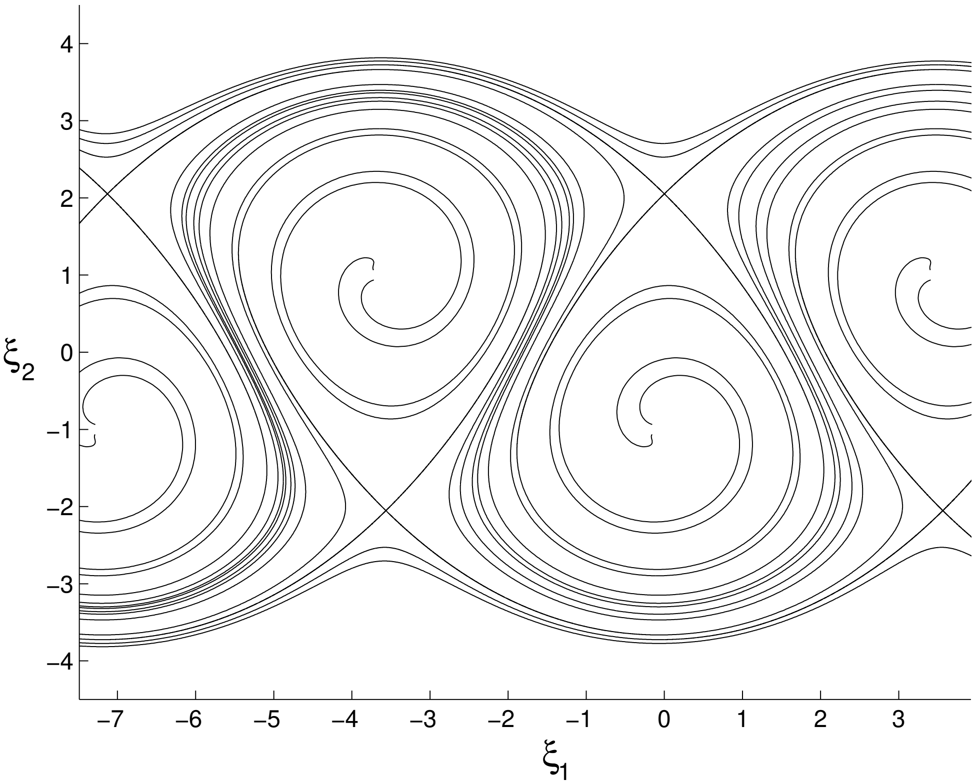

FIG. 11. Incoming and outgoing "whiskers" of several adjacent saddle points in the perturbed motion, with $\epsilon = 0.05$, show that focusing already begins to occur after a particle has advanced by a single period $2p^*$ down the street.

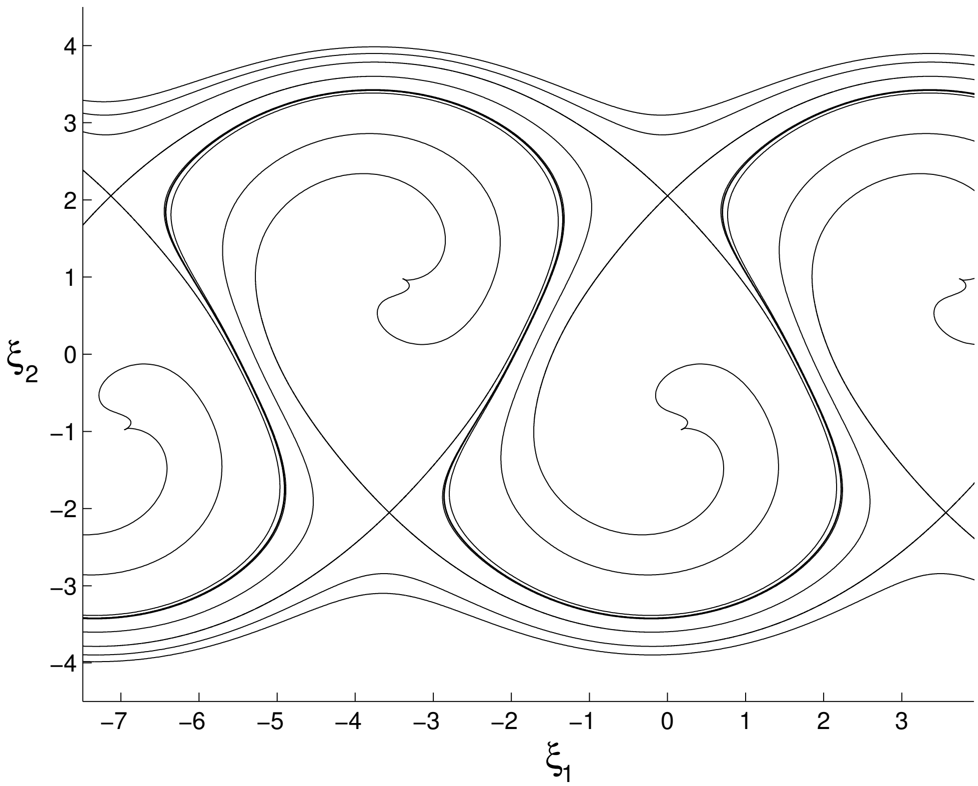

FIG. 12. Incoming and outgoing "whiskers" of several adjacent saddle points in the perturbed motion, with $\epsilon = 0.15$. In this case, particles are already focused into a narrow jet before they advance by a period down the vortex street.

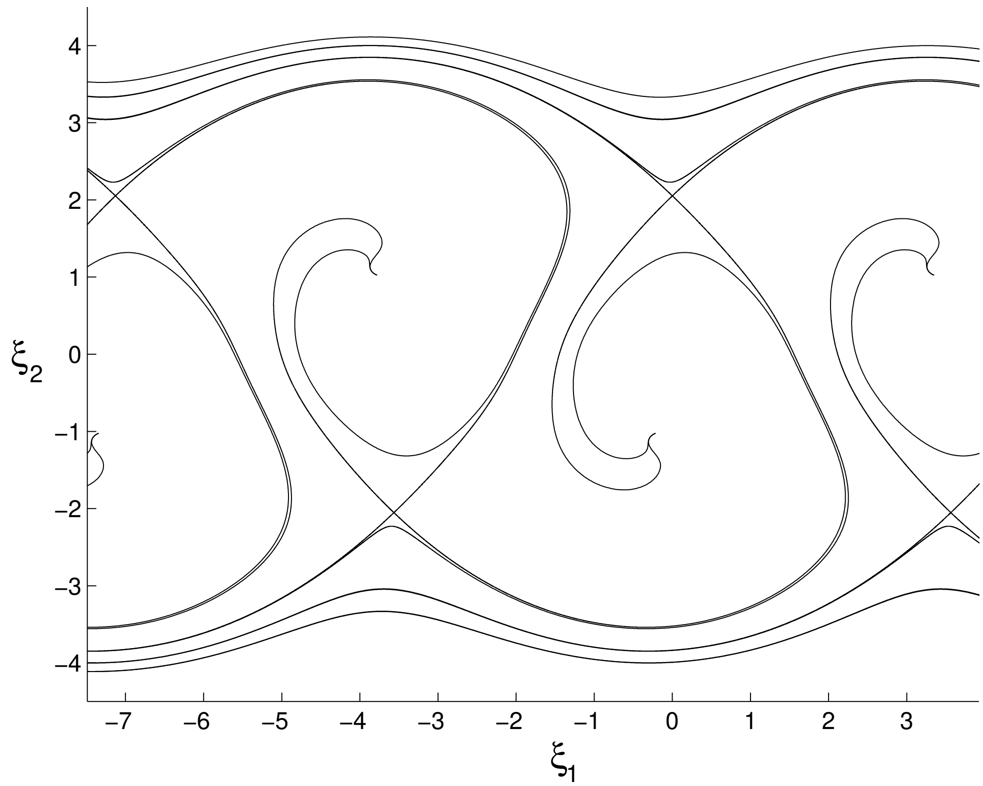

FIG. 13. Incoming and outgoing "whiskers" of several adjacent saddle points in the perturbed motion, with $\epsilon = 0.25$, show the impossibility of any orbits remaining in the vortex street region for $\epsilon \geq 0.25$, because a bifurcation in the qualitative behavior of the separatrices of the saddle points on the slow manifold has taken place.

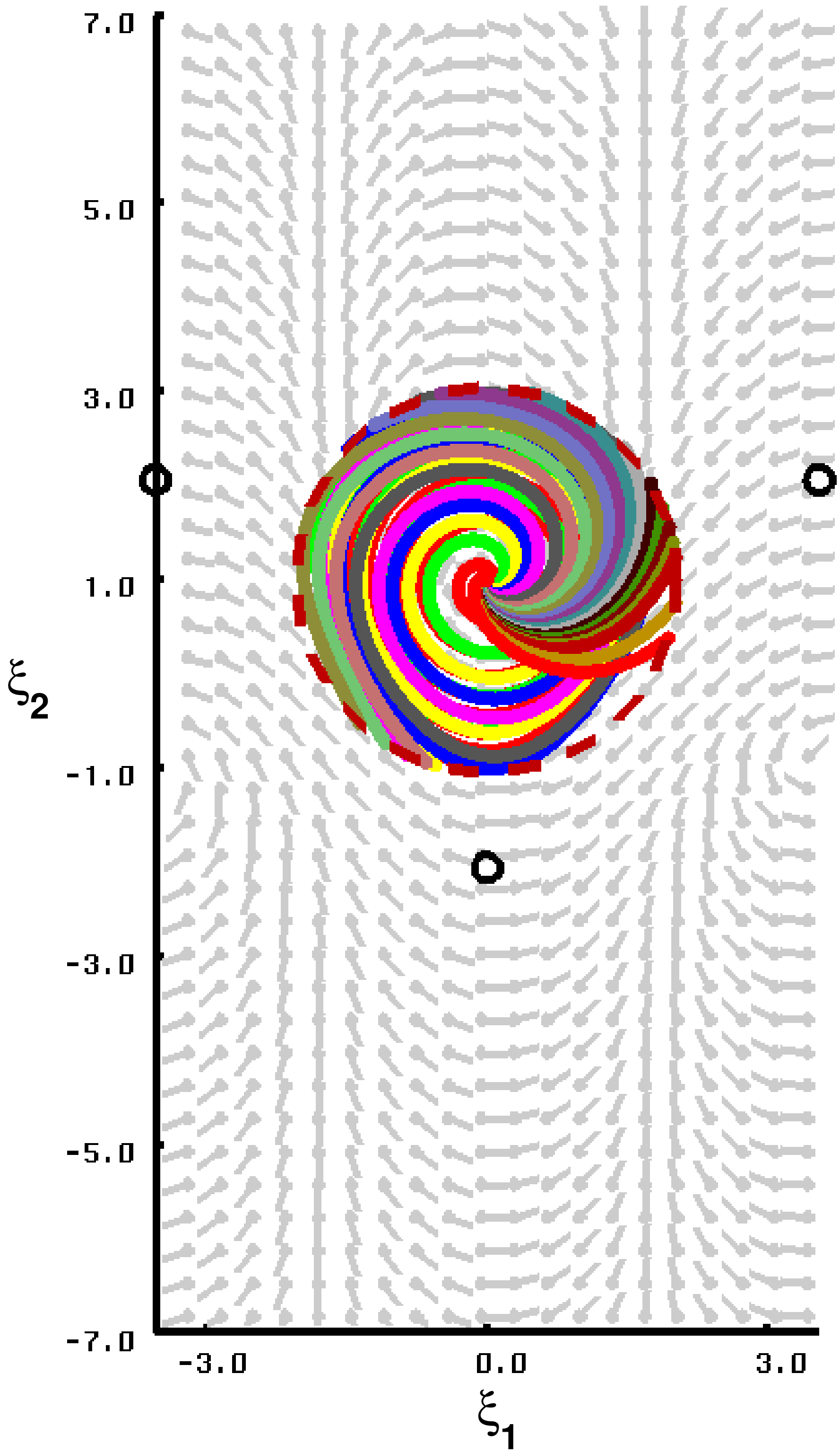

FIG. 14. Particle trajectories terminating at dashed circle for discrete values of ϵ in the range $0.01 < \epsilon < 0.50$. Small circles indicate saddle points in the background flowfield visualized by vectors.

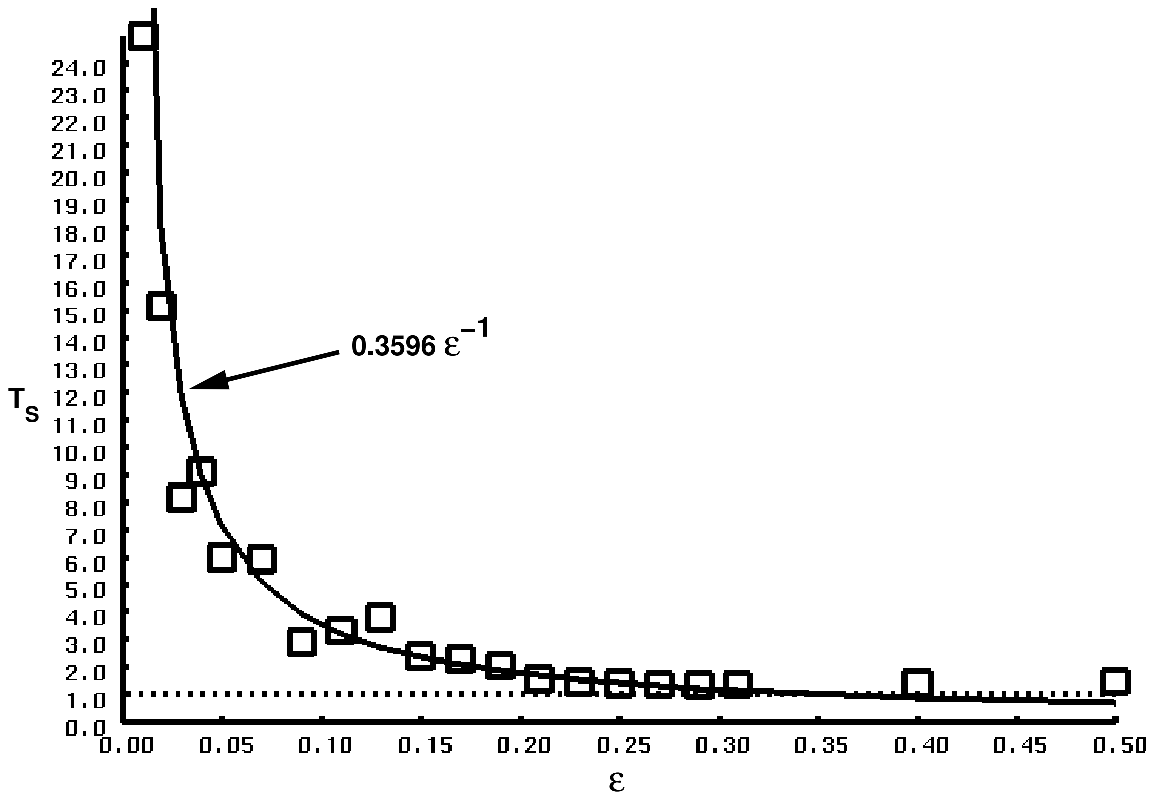

FIG. 15. Normalized spin-out times (square symbols) of particles in the preceding figure as a function of ϵ.

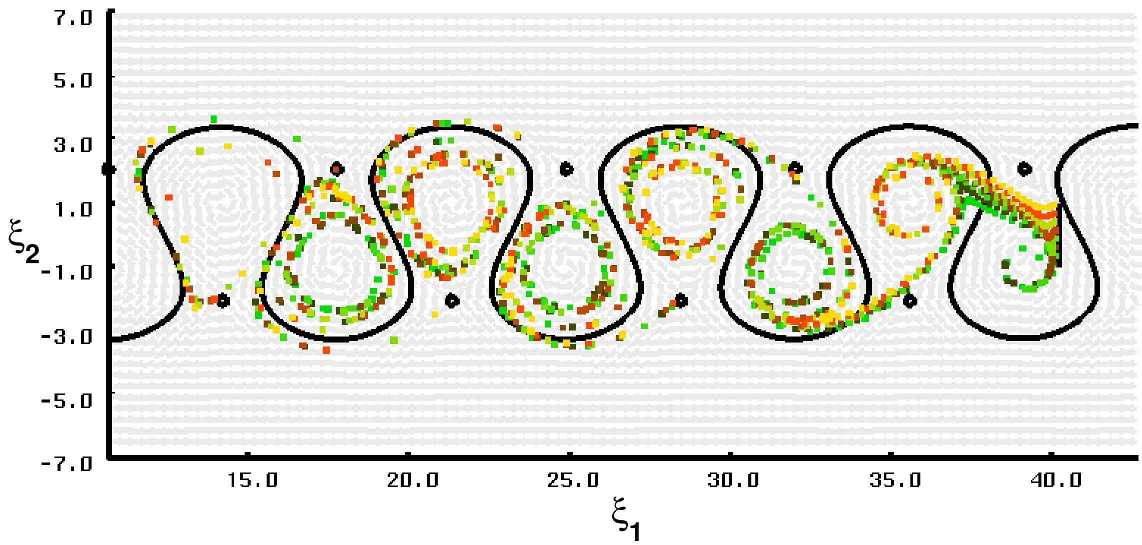

FIG. 16. Streakline plot for $\epsilon = 0.01$ in which a vertical line of length two representing the rear face of a bluff body is moving at four times the street velocity to the right while ejecting particles at zero velocity in the moving frame. The solid line represents the limit cycle of the system on the slow manifold, while the small circles denote saddle points in the background flowfield.

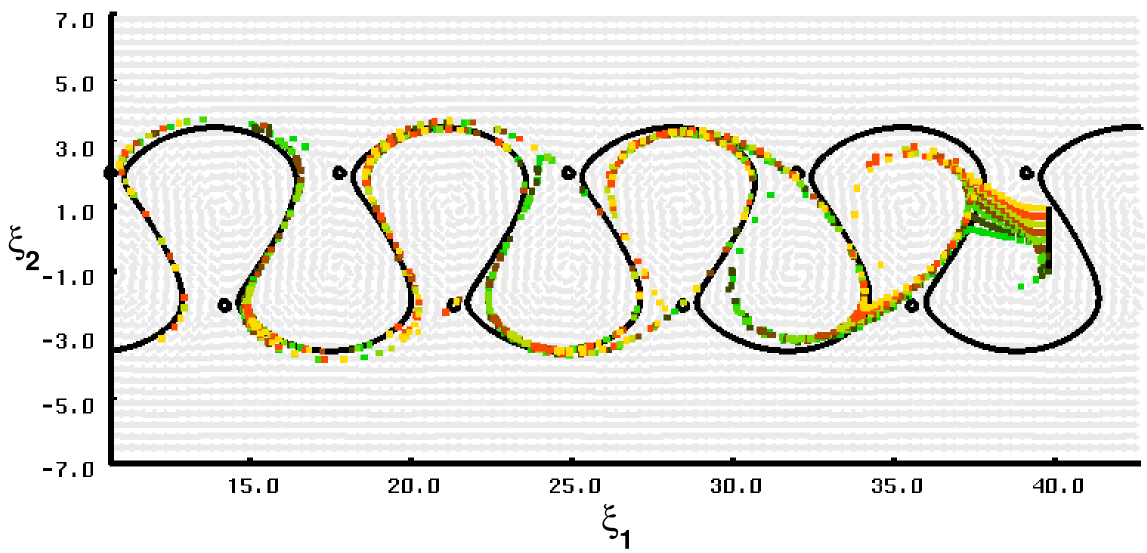

FIG. 17. Streakline plot for $\epsilon = 0.20$. The solid line represents the limit cycle of the system on the slow manifold.

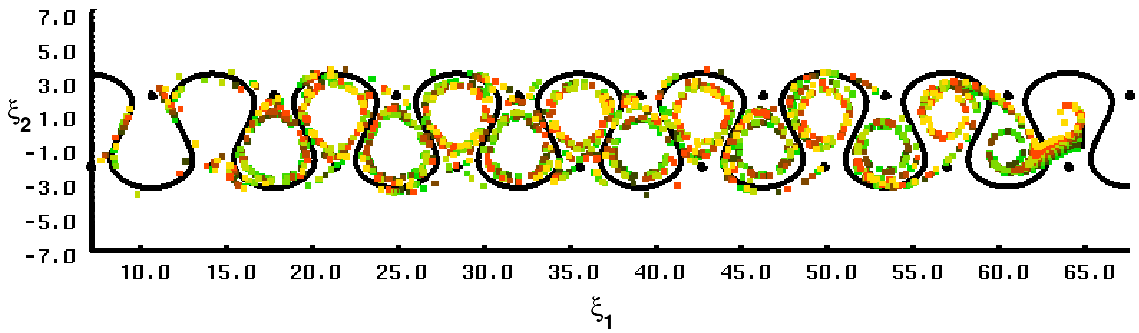

FIG. 18. Streakline plot, as in the preceding two figures, with $\epsilon = 0.015$, showing that particles eventually do spin out to the limit cycle even for small ϵ.